Table 2. Baseline Characteristics of the Study Population

	Kyoto	Kobe City	Fukushima	Total
No. of patients	79	51	37	167
Mean age (yrs)	73.01	70.92	70.64	71.86
Gender				
Women	21 (26.6)	18 (35.3)	8 (21.6)	47 (28.1)
Men	58 (73.4)	33 (64.7)	29 (78.4)	120 (71.9)
Mean visual acuity (logMAR)	0.552	0.605	0.573	0.573
Smoking history				
Never	26 (36.1)	22 (44.9)	15 (40.5)	63 (39.9)
Previous	27 (37.5)	21 (42.9)	12 (32.5)	60 (38.0)
Current	19 (26.4)	6 (12.2)	10 (27.0)	35 (22.1)
Mean follow-up (days)	1156.4	1084.6	1198.8	1143.8
GLD				
≤1800 μm	13 (16.9)	3 (6.3)	7 (18.9)	23 (14.2)
1800–5400 μm	60 (77.9)	41 (85.4)	28 (75.7)	129 (79.6)
>5400 μm	4 (5.2)	4 (8.3)	2 (6.4)	10 (6.2)
Mean (μm)	2817.5	3476.7	3150.5	3209.0

GLD = greatest linear dimension; logMAR = logarithm of the minimal angle of resolution.

based on overall survival analysis (P = 0.214 and 0.166, respectively), although borderline evidence of an association was observed between never smoked and ex-smokers plus current smokers (P = 0.060) (Fig 3).

Effect of Photodynamic Therapy

We investigated the association between the susceptible SNP for the retreatment-free period and initial clinical response to PDT. Of the 167 eyes eligible for this analysis, 13 required additional treatment within 3 months after their first PDT, and 150 did not (Table 4); 4 patients with a follow-up of less than 3 months were excluded. Logistic regression analysis revealed an independent association between SERPINF1 rs12603825 and these subgroups for age, gender, smoking status, and GLD (P = 0.0027). We next conducted a survival analysis of the retreatment-free period in 150 PCV eyes that had been inactivated with a single PDT to evaluate whether this SNP was

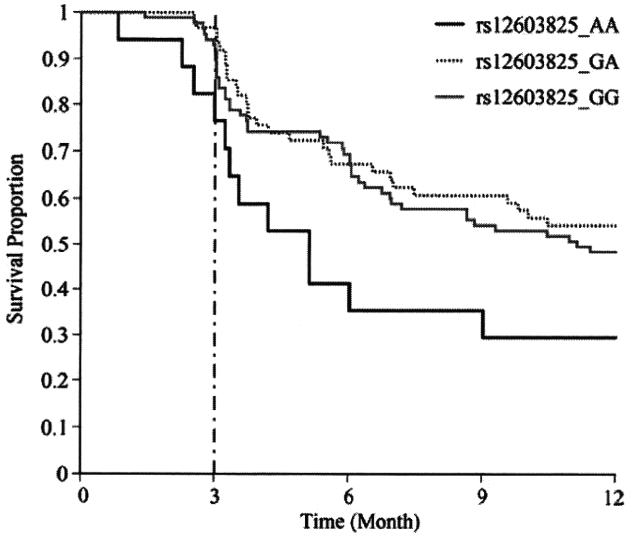

Figure 2. Overall survival analysis curve for the retreatment-free period among patients with the genotype of rs12603825. Patients with AA genotype were administered additional treatment after the first PDT within a significantly shorter period of time than those with other genotypes (P = 0.0038).

associated with recurrence of PCV, but there was no significant difference in the retreatment-free period among genotypes of rs12603825 (P = 0.36), even after adjusting the recessive model (P = 0.16) (Fig 4, available at http://aaojournal.org.).

Visual Outcomes

The visual outcomes after PDT were examined. Seventy-five patients from Kyoto University Hospital were followed up for more than 1 year after their first treatment. Although no significant difference in visual outcomes was observed in lesion size or smoking status (P = 0.523 and 0.468, respectively) (Fig 5, available at http://aaojournal.org.), visual outcomes of patients with the AA genotype of SERPINF1 rs12603825 were significantly worse than those with other genotypes (P = 0.013) (Fig 6).

Table 3. Association Results of Survival Analysis from Screening and Overall Genotyping

						Screening Sample (n = 31)	All Sample (n = 167)		
SNP	Chr*	Position*	Ref.†	Var.†	Gene*	*Corrected P*§	*MAF*	*HWE P*‡	*Nominal P*
rs17732513	14	91456132	C	T	FBLN5	0.000129	0.33	0.39	0.834
rs17793056	3	39284219	C	T	CX3CR1	0.00482	0.31	0.54	0.198
rs12603825	17	1620155	G	A	SERPINF1	0.000195	0.28	0.65	0.0117
rs12103559	17	1622128	G	A	SERPINF1	0.000107	–	–	–
rs1894286	17	1623659	C	T	SERPINF1	0.000162	–	–	–
rs11536889	9	119517952	G	C	TLR4	0.00021	0.23	0.24	0.733
Best-fitting model for significant results									
rs12603825	Recessive model								0.0038

HWE = Hardy–Weinberg equilibrium; MAF = minor allele frequency; SNP = single nucleotide polymorphism.
*Chromosome and position of markers refer to NCBI Build 36.1.
†Ref. and Var. are the reference and variant nucleotides, respectively, that are defined on the reference sequence of NCBI Build 36.1.
‡Hardy–Weinberg equilibrium for genotypic distribution was examined by the Hardy–Weinberg equilibrium exact test.
§*P* value corrected for multiple testing using the Bonferroni method.

Discussion

The present study found a significant association between the SERPINF1 gene variants and the clinical response of PCV to PDT; those patients who were homozygous for the minor allele A of SERPINF1 rs12603825 were administered an additional treatment within a significantly shorter period of time after the first PDT, were significantly less apt to be inactivated by a single treatment (independently of baseline clinical characteristics and smoking status), and had significantly worse visual acuity after PDT than those with no more than 1 copy of the minor allele.

SERPINF1 gene encodes serpin peptidase inhibitor, clade F, member 1, which is also referred to as pigment epithelium-derived factor (PEDF), and was purified first from conditioned medium of human retinal pigment epithelial cells as a factor with potent neural differentiating activity.[27] Subsequent studies have revealed significantly reduced expression of PEDF in retinal pigment epithelial cells, Bruch's membrane,[28,29] and the vitreous[30] of eyes with AMD, whereas other studies have demonstrated the impact of PDT on the expression of PEDF.[31–33] By taking into consideration that PEDF inhibits the migration of endothelial cells in vitro and the in vivo development of experimental retinal neovascularization and choroidal

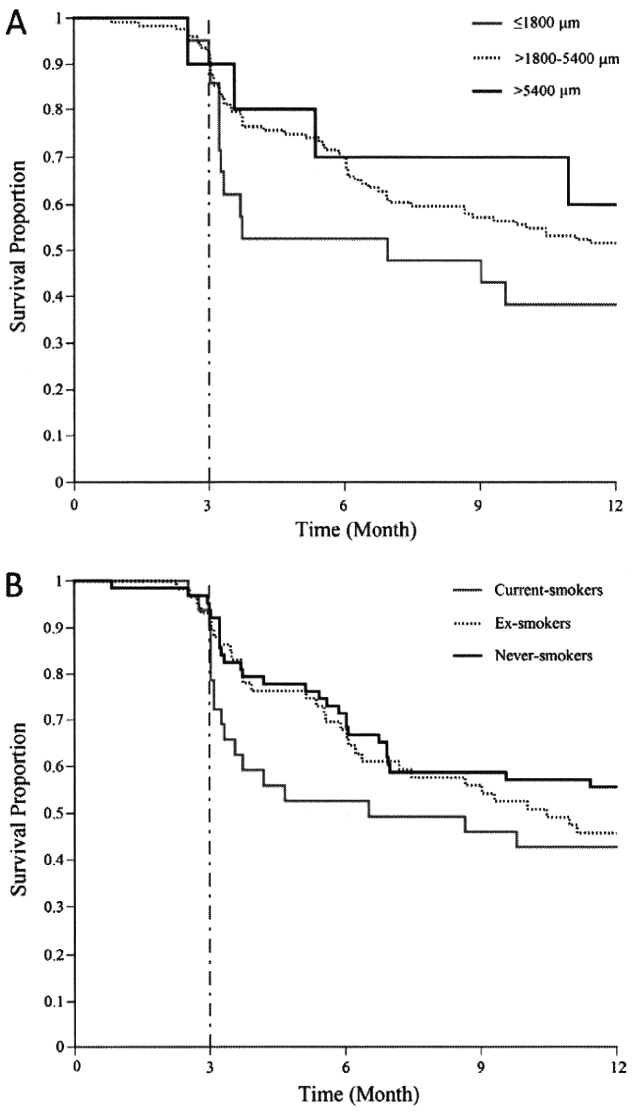

Figure 3. Overall survival analysis curve for the retreatment-free period by the 3 groups of GLD **(A)** and smoking status **(B)**. There was no significant difference among these groups (P = 0.214 and 0.166, respectively), although borderline evidence of an association was observed between those who never smoked and ex-smokers plus current smokers (P = 0.060).

Table 4. Clinical Characteristics and Genotype Distribution of the Study Population by Response to Single Photodynamic Therapy

	Photodynamic Therapy Less Effective*	Photodynamic Therapy Effective*	Adjusted P Value†
No. of patients	13	150	
Mean age (yrs)	69.92	72.19	0.222
Gender			0.283
Women	4 (30.8)	42 (28.0)	
Men	9 (69.2)	108 (72.0)	
Smoking history			0.489
Never	4 (36.4)	59 (41.3)	
Previous	4 (36.4)	55 (38.5)	
Current	3 (27.2)	29 (20.3)	
GLD			0.677
≤1800 μm	2 (15.4)	18 (12.4)	
1800–5400 μm	10 (76.9)	118 (81.4)	
>5400 μm	1 (7.7)	9 (6.2)	
SERPINF1_rs12603825		(GA+GG) vs. AA	0.0027
AA	4 (30.7)	10 (6.8)	
GA	2 (15.4)	60 (40.5)	
GG	7 (53.8)	78 (52.7)	

GLD = greatest linear dimension.
*Patients were divided into 2 subgroups by whether additional treatment was required within the first 3-month follow-up after a single PDT. Less effective = required; effective = not required.
†Adjusted for age, gender, smoking status, greatest linear dimension, and genotype.

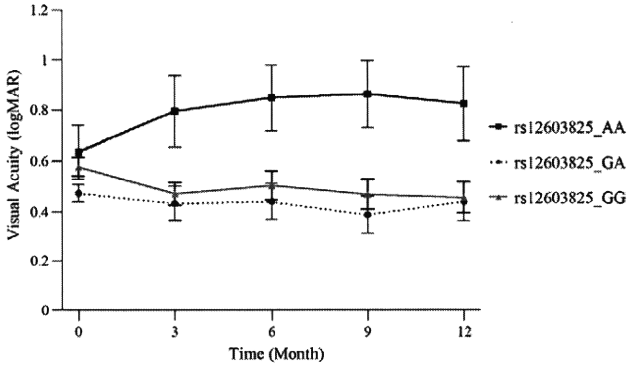

Figure 6. Visual prognosis by SERPINF1 rs12603825 after PDT. Visual outcomes of patients with the AA genotype were significantly worse than those with other genotypes (P = 0.013). Error bars represent ± 1 standard error of the mean. logMAR = logarithm of the minimum angle of resolution.

neovascularization,[34–36] the findings are consistent with those of the present study showing an association between the PEDF gene variants and the response to PDT.

The present study also shows the possibility that PEDF polymorphisms affect PEDF expression in eyes with PCV. We then evaluated whether rs12603825 affects PEDF gene expression in vivo using the raw data deposited in the Gene Expression Omnibus[37] as GSE 6536 (available at: http://www.ncbi.nlm.nih.gov/geo/query/acc.cgi?acc=GSE6536, accessed July 1, 2010). However, there proved to be no association between SERPINF1 rs12603825 and PEDF gene expression (P = 0.689, analysis of variance test), and no significant differences in the baseline clinical characteristics among various genotypes of this SNP (Table 5, available at http://aaojournal.org.). Thus, the PEDF polymorphism may not result in the phenotypic difference via a change in PEDF gene expression. PEDF polymorphisms may influence the binding affinity to the receptor or indirectly affect PEDF expression after PDT by affecting the pathway between PDT and the PDT-induced change of PEDF expression.

As shown by the patients with rs12603825 AA genotype (Fig 1), another possibility regards PEDF polymorphisms as determinants of the probability of hemorrhage after PDT in eyes with PCV, which influences visual prognosis in the long term. All 3 patients with a macular hemorrhage among those who required additional treatment within 3 months after PDT had an rs12603825 AA genotype. Recurrent hemorrhage is one of the most symbolic signs of PCV,[19,21] and visual outcome is poor in eyes that have a massive subretinal hemorrhage involving the macula.[14,38] Furthermore, subretinal hemorrhage after PDT is a common finding in patients with PCV.[39,40] Yokoi et al[41] reported that PEDF levels in vitreous fluid were associated with vitreous hemorrhage in proliferative diabetic retinopathy, but the relationship between hemorrhage and PEDF is not fully understood. With this hypothesis in mind, our study may enhance our understanding of the mechanisms of hemorrhage in PCV.

Previous studies have shown the possibility that small lesions in patients with AMD respond better to PDT than larger lesions,[10,42] but the current study found no significant association between baseline lesion size and response to PDT. Conversely, we found that individuals who never smoked were less prone to recurrence than ex-smokers or current smokers. This result seems to be in agreement with the numerous studies that have shown smoking to be a risk factor for the development of AMD[43–46] and that smoking strongly influences the development of PCV.[18–20]

Study Limitations

One limitation of the present study is the number of participants. We found no significant association between rs12603825 and the retreatment-free period in eyes with PCV that responded to a single administration of PDT, although patients homozygous for the minor allele did tend to be administered additional treatment within a shorter period of time than those with other genotypes in the long term (Fig 4, available at http://aaojournal.org.). This tendency might reach statistical significance if the number of patients were increased. Other reports have demonstrated an association between the initial response and the risk of recurrence in other diseases.[47,48] Another limitation is the subgroup that initially responded to PDT may not represent a true difference in histologic response to PDT, because this relied on clinical information. Further basic research is needed to better characterize the relationship between the PEDF gene and the response to PDT. Another limitation is the absence of evaluation for the response to repeated treatments of PDT. Approximately half of the patients who noted less-effective responses to the first PDT received other treatments (e.g., anti-VEGF therapy or combined treatment) as their additional therapy. Further validation studies (e.g., prospective study) are obviously needed to clarify the detailed clinical response to PDT.

In conclusion, this study provides the first evidence that clinical, environmental, and genetic factors influence the response of PCV to PDT: PEDF gene variants associate independently with their response to PDT. Although it remains controversial as to whether PCV represents a subtype of neovascular AMD, the response to PDT is completely different for PCV and for neovascular AMD. Intravitreal injection of adenoviral vectors containing PEDF complementary DNA has been suggested to be a viable approach to therapy for neovascular AMD;[49,50] thus, our findings may lead to ways to modify the effects of PDT, to new methods of treatment using these materials, and to an understanding of the pathogenesis of PCV.

References

1. Sho K, Takahashi K, Yamada H, et al. Polypoidal choroidal vasculopathy: incidence, demographic features, and clinical characteristics. Arch Ophthalmol 2003;121:1392–6.
2. Maruko I, Iida T, Saito M, et al. Clinical characteristics of exudative age-related macular degeneration in Japanese patients. Am J Ophthalmol 2007;144:15–22.
3. Ciardella AP, Donsoff IM, Huang SJ, et al. Polypoidal choroidal vasculopathy. Surv Ophthalmol 2004;49:25–37.
4. Edwards AO, Ritter R III, Abel KJ, et al. Complement factor H polymorphism and age-related macular degeneration. Science 2005;308:421–4.
5. Gotoh N, Nakanishi H, Hayashi H, et al. *ARMS2* (*LOC387715*) variants in Japanese patients with exudative age-related macular degeneration and polypoidal choroidal vasculopathy. Am J Ophthalmol 2009;147:1037–41.
6. Gotoh N, Yamada R, Nakanishi H, et al. Correlation between *CFH* Y402H and *HTRA1* rs11200638 genotype to typical exudative age-related macular degeneration and polypoidal choroidal vasculopathy phenotype in the Japanese population. Clin Experiment Ophthalmol 2008;36:437–42.
7. Gotoh N, Kuroiwa S, Kikuchi T, et al. Apolipoprotein E polymorphisms in Japanese patients with polypoidal choroidal vasculopathy and exudative age-related macular degeneration. Am J Ophthalmol 2004;138:567–73.
8. Seddon JM, Reynolds R, Maller J, et al. Prediction model for prevalence and incidence of advanced age-related macular degeneration based on genetic, demographic, and environmental variables. Invest Ophthalmol Vis Sci 2009;50:2044–53.
9. Treatment of Age-Related Macular Degeneration With Photodynamic Therapy Study Group. Verteporfin therapy of

subfoveal choroidal neovascularization in patients with age-related macular degeneration: additional information regarding baseline lesion composition's impact on vision outcomes-TAP report no. 3. Arch Ophthalmol 2002;120: 1443–54.
10. Arias L, Pujol O, Berniell J, et al. Impact of lesion size on photodynamic therapy with verteporfin of predominantly classic lesions in age related macular degeneration. Br J Ophthalmol 2005;89:312–5.
11. Immonen I, Seitsonen S, Tommila P, et al. Vascular endothelial growth factor gene variation and the response to photodynamic therapy in age-related macular degeneration. Ophthalmology 2010;117:103–8.
12. Feng X, Xiao J, Longville B, et al. Complement factor H Y402H and C-reactive protein polymorphism and photodynamic therapy response in age-related macular degeneration. Ophthalmology 2009;116:1908–12.
13. Spaide RF, Donsoff I, Lam DL, et al. Treatment of polypoidal choroidal vasculopathy with photodynamic therapy. Retina 2002;22:529–35.
14. Gomi F, Ohji M, Sayanagi K, et al. One-year outcomes of photodynamic therapy in age-related macular degeneration and polypoidal choroidal vasculopathy in Japanese patients. Ophthalmology 2008;115:141–6.
15. Tsuchiya D, Yamamoto T, Kawasaki R, Yamashita H. Two-year visual outcomes after photodynamic therapy in age-related macular degeneration patients with or without polypoidal choroidal vasculopathy lesions. Retina 2009;29:960–5.
16. Yamashiro K, Tsujikawa A, Nishida A, et al. Recurrence of polypoidal choroidal vasculopathy after photodynamic therapy. Jpn J Ophthalmol 2008;52:457–62.
17. Kurashige Y, Otani A, Sasahara M, et al. Two-year results of photodynamic therapy for polypoidal choroidal vasculopathy. Am J Ophthalmol 2008;146:513–9.
18. Kikuchi M, Nakamura M, Ishikawa K, et al. Elevated C-reactive protein levels in patients with polypoidal choroidal vasculopathy and patients with neovascular age-related macular degeneration. Ophthalmology 2007;114:1722–7.
19. Laude A, Cackett PD, Vithana EN, et al. Polypoidal choroidal vasculopathy and neovascular age-related macular degeneration: same or different disease? Prog Retin Eye Res 2010;29: 19–29.
20. Nakanishi H, Yamashiro K, Yamada R, et al. Joint effect of cigarette smoking, *CFH* and *LOC387715/HTRA1* polymorphisms on polypoidal choroidal vasculopathy. Invest Ophthalmol Vis Sci 2010;51:6183–7. Epub 2010 Aug 4.
21. Japanese Study Group of Polypoidal Choroidal Vasculopathy. Criteria for diagnosis of polypoidal choroidal vasculopathy [in Japanese]. Nippon Ganka Gakkai Zasshi 2005;109:417–27.
22. Otani A, Sasahara M, Yodoi Y, et al. Indocyanine green angiography: guided photodynamic therapy for polypoidal choroidal vasculopathy. Am J Ophthalmol 2007;144:7–14.
23. Treatment of Age-Related Macular Degeneration with Photodynamic Therapy (TAP) Study Group. Photodynamic therapy of subfoveal choroidal neovascularization in age-related macular degeneration with verteporfin: one-year results of 2 randomized clinical trials—TAP report 1. Arch Ophthalmol 1999;117:1329–45.
24. Tano Y, Ophthalmic PDT Study Group. Guidelines for PDT in Japan [letter]. Ophthalmology 2008;115:585.
25. Chan WM, Lam DS, Lai TY, et al. Photodynamic therapy with verteporfin for symptomatic polypoidal choroidal vasculopathy: one-year results of a prospective case series. Ophthalmology 2004;111:1576–84.
26. Barrett JC, Fry B, Maller J, Daly MJ. Haploview: analysis and visualization of LD and haplotype maps. Bioinformatics 2005; 21:263–5.
27. Tombran-Tink J, Chader GG, Johnson LV. PEDF: a pigment epithelium-derived factor with potent neuronal differentiative activity [letter]. Exp Eye Res 1991;53:411–4.
28. Bhutto IA, Uno K, Merges C, et al. Reduction of endogenous angiogenesis inhibitors in Bruch's membrane of the submacular region in eyes with age-related macular degeneration. Arch Ophthalmol 2008;126:670–8.
29. Bhutto IA, McLeod DS, Hasegawa T, et al. Pigment epithelium-derived factor (PEDF) and vascular endothelial growth factor (VEGF) in aged human choroid and eyes with age-related macular degeneration. Exp Eye Res 2006;82:99–110.
30. Holekamp NM, Bouck N, Volpert O. Pigment epithelium-derived factor is deficient in the vitreous of patients with choroidal neovascularization due to age-related macular degeneration. Am J Ophthalmol 2002;134:220–7.
31. Schmidt-Erfurth U, Schlotzer-Schrehard U, Cursiefen C, et al. Influence of photodynamic therapy on expression of vascular endothelial growth factor (VEGF), VEGF receptor 3, and pigment epithelium-derived factor. Invest Ophthalmol Vis Sci 2003;44:4473–80.
32. Tatar O, Adam A, Shinoda K, et al. Expression of VEGF and PEDF in choroidal neovascular membranes following verteporfin photodynamic therapy. Am J Ophthalmol 2006;142:95–104.
33. Obata R, Iriyama A, Inoue Y, et al. Triamcinolone acetonide suppresses early proangiogenic response in retinal pigment epithelial cells after photodynamic therapy in vitro. Br J Ophthalmol 2007;91:100–4.
34. Dawson DW, Volpert OV, Gillis P, et al. Pigment epithelium-derived factor: a potent inhibitor of angiogenesis. Science 1999;285:245–8.
35. Mori K, Duh E, Gehlbach P, et al. Pigment epithelium-derived factor inhibits retinal and choroidal neovascularization. J Cell Physiol 2001;188:253–63.
36. Mori K, Gehlbach P, Yamamoto S, et al. AAV-mediated gene transfer of pigment epithelium-derived factor inhibits choroidal neovascularization. Invest Ophthalmol Vis Sci 2002;43: 1994–2000.
37. Edgar R, Domrachev M, Lash AE. Gene Expression Omnibus: NCBI gene expression and hybridization array data repository. Nucleic Acids Res 2002;30:207–10.
38. Jalali S, Parra SL, Majji AB, et al. Ultrasonographic characteristics and treatment outcomes of surgery for vitreous hemorrhage in idiopathic polypoidal choroidal vasculopathy. Am J Ophthalmol 2006;142:608–19.
39. Hirami Y, Tsujikawa A, Otani A, et al. Hemorrhagic complications after photodynamic therapy for polypoidal choroidal vasculopathy. Retina 2007;27:335–41.
40. Ojima Y, Tsujikawa A, Otani A, et al. Recurrent bleeding after photodynamic therapy in polypoidal choroidal vasculopathy. Am J Ophthalmol 2006;141:958–60.
41. Yokoi M, Yamagishi S, Saito A, et al. Positive association of pigment epithelium-derived factor with total antioxidant capacity in the vitreous fluid of patients with proliferative diabetic retinopathy. Br J Ophthalmol 2007;91:885–7.
42. Verteporfin In Photodynamic Therapy Study Group. Verteporfin therapy of subfoveal choroidal neovascularization in age-related macular degeneration: two-year results of a randomized clinical trial including lesions with occult with no classic choroidal neovascularization—Verteporfin in Photodynamic Therapy report 2. Am J Ophthalmol 2001;131: 541–60.

43. Eye Disease Case-Control Study Group. Risk factors for neovascular age-related macular degeneration. Arch Ophthalmol 1992;110:1701–8.
44. Christen WG, Glynn RJ, Manson JE, et al. A prospective study of cigarette smoking and risk of age-related macular degeneration in men. JAMA 1996;276:1147–51.
45. Seddon JM, Willett WC, Speizer FE, Hankinson SE. A prospective study of cigarette smoking and age-related macular degeneration in women. JAMA 1996;276:1141–6.
46. Hyman LG, Lilienfeld AM, Ferris FL III, Fine SL. Senile macular degeneration: a case-control study. Am J Epidemiol 1983;118:213–27.
47. Huber KE, Carey LA, Wazer DE. Breast cancer molecular subtypes in patients with locally advanced disease: impact on prognosis, patterns of recurrence, and response to therapy. Semin Radiat Oncol 2009;19:204–10.
48. Van den Eynde E, Tiraboschi JM, Tural C, et al. Ability of treatment week 12 viral response to predict long-term outcome in genotype 1 hepatitis C virus/HIV coinfected patients. AIDS 2010;24:975–82.
49. Campochiaro PA, Nguyen QD, Shah SM, et al. Adenoviral vector-delivered pigment epithelium-derived factor for neovascular age-related macular degeneration: results of a phase I clinical trial. Hum Gene Ther 2006;17:167–76.
50. Imai D, Yoneya S, Gehlbach PL, et al. Intraocular gene transfer of pigment epithelium-derived factor rescues photoreceptors from light-induced cell death. J Cell Physiol 2005; 202:570–8.

Footnotes and Financial Disclosures

Originally received: August 13, 2010.
Final revision: November 10, 2010.
Accepted: December 10, 2010.
Available online: ●●●. Manuscript no. 2010-1115.

[1] Department of Ophthalmology, Kyoto University Graduate School of Medicine, Kyoto, Japan.

[2] Center for Genomic Medicine/Inserm U.852, Kyoto University Graduate School of Medicine, Kyoto, Japan.

[3] Department of Ophthalmology, Fukushima Medical University, Fukushima, Japan.

[4] Department of Ophthalmology, Kobe City Medical Center General Hospital, Kobe, Japan.

Presented at: The American Academy of Ophthalmology Annual Meeting, October 16–19, 2010, Chicago, Illinos.

Financial Disclosure(s):
The author(s) have no proprietary or commercial interest in any materials discussed in this article.

Supported in part by grants-in-aid for scientific research (Nos. 21249084 and 200791294) from the Japan Society for the Promotion of Science, Tokyo, Japan, and the Japan National Society for the Prevention of Blindness, Tokyo, Japan. The funding organizations had no role in the design or conduct of this research.

Correspondence:
Kenji Yamashiro, MD, PhD, Department of Ophthalmology and Visual Sciences, Kyoto University Graduate School of Medicine, 54 Kawahara, Shogoin, Sakyo, Kyoto 606-8507, Japan. E-mail: yamashro@kuhp.kyoto-u.ac.jp.

OPEN ACCESS Freely available online

PLoS one

The Progression of Liver Fibrosis Is Related with Overexpression of the miR-199 and 200 Families

Yoshiki Murakami[1]*, Hidenori Toyoda[2], Masami Tanaka[3], Masahiko Kuroda[3], Yoshinori Harada[4], Fumihiko Matsuda[1], Atsushi Tajima[5¤], Nobuyoshi Kosaka[6], Takahiro Ochiya[6], Kunitada Shimotohno[7]

1 Center for Genomic Medicine, Kyoto University Graduate School of Medicine, Kyoto, Japan, **2** Department of Gastroenterology, Ogaki Municipal Hospital, Ogaki, Japan, **3** Department of Molecular Pathology, Tokyo Medical University, Tokyo, Japan, **4** Department of Pathology and Cell Regulation, Kyoto Prefectural University of Medicine, Kyoto, Japan, **5** Department of Molecular Life Science, Tokai University School of Medicine, Isehara, Japan, **6** Division of Molecular and Cellular Medicine, National Cancer Center Research Institute, Tokyo, Japan, **7** Research Institute, Chiba Institute of Technology, Narashino, Japan

Abstract

Background: Chronic hepatitis C (CH) can develop into liver cirrhosis (LC) and hepatocellular carcinoma (HCC). Liver fibrosis and HCC development are strongly correlated, but there is no effective treatment against fibrosis because the critical mechanism of progression of liver fibrosis is not fully understood. microRNAs (miRNAs) are now essential to the molecular mechanisms of several biological processes. In order to clarify how the aberrant expression of miRNAs participates in development of the liver fibrosis, we analyzed the liver fibrosis in mouse liver fibrosis model and human clinical samples.

Methodology: In a CCL_4-induced mouse liver fibrosis model, we compared the miRNA expression profile from CCL_4 and olive oil administrated liver specimens on 4, 6, and 8 weeks. We also measured expression profiles of human miRNAs in the liver biopsy specimens from 105 CH type C patients without a history of anti-viral therapy.

Principle Findings: Eleven mouse miRNAs were significantly elevated in progressed liver fibrosis relative to control. By using a large amount of human material in CH analysis, we determined the miRNA expression pattern according to the grade of liver fibrosis. We detected several human miRNAs whose expression levels were correlated with the degree of progression of liver fibrosis. In both the mouse and human studies, the expression levels of miR-199a, 199a*, 200a, and 200b were positively and significantly correlated to the progressed liver fibrosis. The expression level of fibrosis related genes in hepatic stellate cells (HSC), were significantly increased by overexpression of these miRNAs.

Conclusion: Four miRNAs are tightly related to the grade of liver fibrosis in both human and mouse was shown. This information may uncover the critical mechanism of progression of liver fibrosis. miRNA expression profiling has potential for diagnostic and therapeutic applications.

Citation: Murakami Y, Toyoda H, Tanaka M, Kuroda M, Harada Y, et al. (2011) The Progression of Liver Fibrosis Is Related with Overexpression of the miR-199 and 200 Families. PLoS ONE 6(1): e16081. doi:10.1371/journal.pone.0016081

Editor: Chad Creighton, Baylor College of Medicine, United States of America

Received September 15, 2010; **Accepted** December 6, 2010; **Published** January 24, 2011

Funding: This work was supported by the Japanese Ministry of Health, Labour and Welfare (Y.M, and K.S). This work was also supported by the 'Strategic Research-Based Support' Project for private universities; with matching funds from the Ministry of Education, Culture, Sports, Science and Technology (M.K). The funders had no role in study design, data collection and analysis, decision to publish, or preparation of the manuscript.

Competing Interests: The authors have declared that no competing interests exist.

* E-mail: ymurakami@genome.med.kyoto-u.ac.jp

¤ Current address: Department of Human Genetics and Public Health, Institute of Health Biosciences, The University of Tokushima Graduate School, Tokushima, Japan

Introduction

Chronic viral hepatitis is a major risk factor for hepatocellular carcinoma (HCC) [1]. Worldwide 120–170 million persons are currently chronically Hepatitis C Virus (HCV) infected [2]. Due to repetitive and continuous inflammation, these patients are at increased risk of developing cirrhosis, subsequent liver decompensation and/or hepatocellular carcinoma. However, the current standard of care; pegylated interferon and rivabirin combination therapy is unsatisfied in the patients with high titre of HCVRNA and genotype 1b. Activated human liver stellate cells (HSC) with chronic viral infection, can play a pivotal role in the progression of liver fibrosis [3]. Activated HSC produce a number of profibrotic cytokines and growth factors that perpetuate the fibrotic process through paracrine and autocrine effects.

MicroRNAs (miRNAs) are endogenous small non-coding RNAs that control gene expression by degrading target mRNA or suppressing their translation [4]. There are currently 940 identifiable human miRNAs (The miRBase Sequence Database - Release ver. 15.0). miRNAs can recognize hundreds of target genes with incomplete complementary; over one third of human genes appear to be conserved miRNA targets [5][6]. miRNA is associated several pathophysiologic events as well as fundamental cellular processes such as cell proliferation and differentiation. Aberrant expression of miRNA can be associated with the liver diseases [7][8][9][10]. Recently reported miRNAs can regulate the activation of HSCs and thereby regulate liver fibrosis. miR-29b, a negative regulator for the type I collagen and SP1, is a key regulator of liver fibrosis [11]. miR-27a and 27b allowed culture-activated rat HSCs to switch to a more quiescent HSC phenotype,

with restored cytoplasmic lipid droplets and decreased cell proliferation [12].

In this study, we aimed to reveal the association between miRNA expression patterns and the progression of liver fibrosis by using a chronic liver inflammation model in mouse. We also sought to identify the miRNA expression profile in chronic hepatitis (CH) C patients according to the degree of liver fibrosis, and to clarify how miRNAs contribute to the progression of liver fibrosis. We observed a characteristic miRNA expression profile common to both human liver biopsy specimens and mouse CCL_4 specimens, comprising the key miRNAs which are associated with the liver fibrosis. This information is expected to uncover the mechanism of liver fibrosis and to provide a clearer biomarker for diagnosis of liver fibrosis as well as to aid in the development of more effective and safer therapeutic strategies for liver fibrosis.

Results

The expression level of several mouse miRNAs was increased by introducing mouse liver fibrosis

In order to identify changes in the miRNA expression profile between advanced liver fibrosis and non-fibrotic liver, we intraperitoneally administered CCL_4 in olive oil or olive oil alone twice a week for 4 weeks and then once a week for the next 4 weeks. Mice were sacrificed at 4, 6, or 8 weeks and then the degree of mouse liver fibrosis was determined by microscopy (Figure S1). miRNA expression analysis was performed from the liver tissue collected at the same time. Histological examination revealed that the degree of liver fibrosis progressed in mice that received CCL_4 relative to mice receiving olive oil alone (Figure 1A). Microarray analysis revealed that in CCL_4 mice, the expression level of 11 miRNAs was consistently higher than that in control mice (Figure 1B).

miRNA expression profile in each human liver fibrosis grade

We then established human miRNAs expression profile by using 105 fresh-frozen human chronic hepatitis (CH) C liver tissues without a history of anti-viral therapy, classified according to the grade of the liver fibrosis (F0, F1, F2, and F3 referred to METAVIR fibrosis stages)(Figure 2, Table S2). Fibrosis grade F0 was considered to be the negative control because these samples were derived from patients with no finding of liver fibrosis. In zebrafish, most highly tissue-specific miRNAs are expressed during embryonic development; approximately 30% of all miRNAs are expressed at a given time point in a given tissue [13]. In mammals, the 20–30% miRNA call rate has recently been validated [14]. Such analysis revealed that the diversity of miRNA expression level among specimens was small. Therefore, we focused on miRNAs with a fold change in mean expression level greater than 1.5 ($p<0.05$) in the two arbitrary groups of liver fibrosis.

Expression of several miRNAs was dramatically different among grades of fibrosis. In the mice study 11 miRNAs were related to the progression of liver fibrosis (mmu-let-7e, miR-125-5p, 199a-5p, 199b, 199b*, 200a, 200b, 31, 34a, 497, and 802). In the human study 10 miRNAs were extracted, and the change in their expression level varied significantly between F0 and F3 (F0<F3: hsa-miR-146b, 199a, 199a*, 200a, 200b, 34a, and 34b, F0>F3: hsa-miR-212, 23b, and 422b). The expression level of 6 miRNAs was significantly different between F0 and F2 (F0<F2: hsa-miR-146b, 200a, 34a, and 34b, F0>F2: hsa-miR-122 and 23b). 5 extracted miRNAs had an expression level that was significantly different between F1 and F2 (F1<F2: hsa-miR-146b, F1>F2: hsa-miR-122, 197, 574, and 768-5p). The expression level of 9 miRNAs changed significantly between F1 and F3 (F1<F3: hsa-miR-146b, 150, 199a, 199a*, 200a, and 200b, F1>F3: hsa-miR-378, 422b, and 768-5p). The miRNAs related to liver fibrosis were extracted using two criteria: similar expression pattern in both the human and the mice specimens and shared sequence between human and mouse. We compared the sequences of mouse miRNAs as described on the Agilent Mouse MiRNA array Version 1.0 (miRbase Version 10.1) and human miRNAs as described on the Agilent Human MiRNA array Version 1.5 (miRbase Version 9.1). The sequences of mmu-miR-199a-5p, mmu-miR-199b, mmu-miR-199b, mmu-miR-200a, and mmu-miR-200b in mouse miRNA corresponded to the sequences of hsa-miR-199a, hsa-miR-199a*, hsa-miR-199a, hsa-miR-200a, and hsa-miR-200b in human miRNA, respectively (Table S3).

Validation of the microarray result by real-time qPCR

The 4 human miRNAs (miR-199a, miR-199a*, miR-200a, and miR-200b) with the largest difference in fold change between the F1 and F3 groups were chosen to validate the microarray results using stem-loop based real-time qPCR. The result of real-time qPCR supported the result of that microarray analysis. The expression level of these 4 miRNAs was significantly different between F0 and F3 and spearman correlation analysis also showed that the expressions of these miRNAs were strongly and positively correlated with fibrosis grade ($n = 105$, $r = 0.498$(miR-199a), 0.607(miR-199a*), 0.639(miR-200a), 0.618(miR-200b), p-values<0.0001) (Figure 3).

Over expression of miR-199a, 199a*, 200a, and 200b was associated with the progression of liver fibrosis

In order to reveal the function of miR-199a, miR-199a*, miR-200a, and miR-200b, we investigated the involvement of these miRNAs in the modulation of fibrosis-related gene in LX-2 cells. The endogenous expression level of these 4 miRNAs in LX2 and normal liver was low according to the microarray study (Figure S2). Transforming growth factor (TGF)β is one of the critical factors for the activation of HSC during chronic inflammation [15] and TGFβ strongly induced expression of three fibrosis-related genes include a matrix degrading complex comprised of α1 procollagen, matrix remodeling complex, comprised of metalloproteinases-13 (MMP-13), tissue inhibitors of metalloproteinases-1 (TIMP-1) in LX-2 cells (Figure 4A). Furthermore, overexpression of miR-199a, miR-199a*, miR-200a and miR-200b in LX-2 cells resulted significant induction of above fibrosis-related genes compared with control miRNA (Figure 4B). Finally we validated the involvement of TGFβ in the modulation of these miRNAs. In LX-2 cells treated with TGFβ, the expression levels of miR-199a and miR-199a* were significantly higher than in untreated cells; the expression levels of miR-200a and miR-200b were significantly lower than in untreated cells. Thus, our in vitro analysis suggested a possible involvement of miR-199a, 199a*, 200a, and 200b in the progression of liver fibrosis.

Discussion

Our comprehensive analysis showed that the aberrant expression of miRNAs was associated with the progression of liver fibrosis. We identified that 4 highly expressed miRNAs (miR-199a, miR-199a*, miR-200a, and miR-200b) that were significantly associated with the progression of liver fibrosis both human and mouse. Coordination of aberrant expression of these miRNAs may contribute to the progression of liver fibrosis.

Prior studies have discussed the expression pattern of miRNA found in liver fibrosis samples between previous and present study. In this report and prior mouse studies and the expression pattern of

A

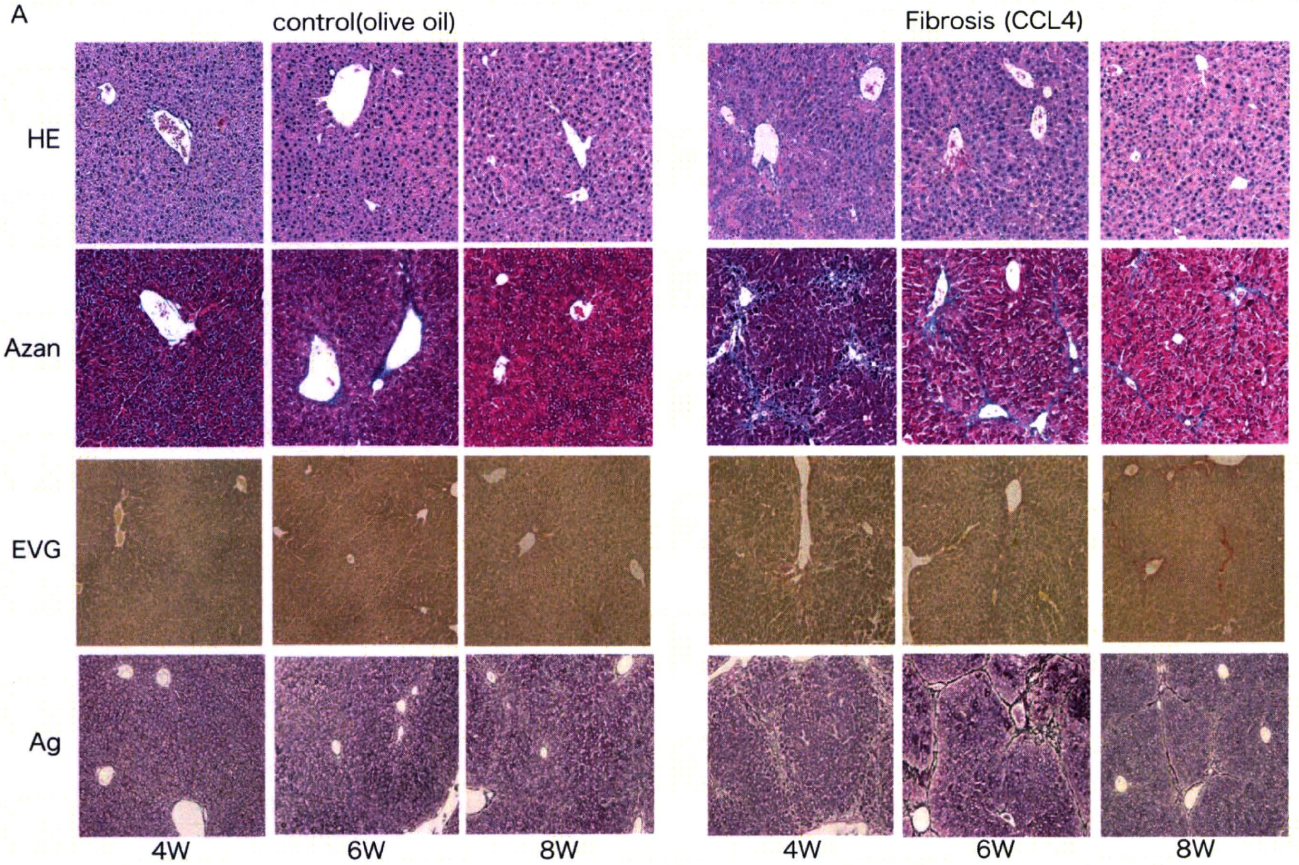

B

miRNA	Fold change CCL4 mouse/control		
	4week	6week	8week
mmu-let-7e	2.92	2.09	2.64
mmu-miR-125a-5p	4.29	2.35	2.67
mmu-miR-199a-5p	2.71	2.12	2.38
mmu-miR-199b	3.25	2.55	2.49
mmu-miR-199b*	5.13	4.47	3.94
mmu-miR-200a	2.23	1.63	2.02
mmu-miR-200b	2.38	2.06	2.20
mmu-miR-31	3.4	2.35	3.19
mmu-miR-34a	3.89	3.22	3.5
mmu-miR-497	2.25	2.00	2.55
mmu-miR-802	2.02	2.87	2.74

Figure 1. The change of liver fibrosis in mouse model. A. Representative H&E-stained, Azan-stained, Ag-stained, and EVG-stained histological sections of liver from mice receiving olive oil alone or CCL_4 in olive oil. Magnification is ×10. B. The expression level of mmu-miRNA in mouse liver with olive oil or CCL_4 at 4W, 6W, and 8W respectively, by microarray analysis.
doi:10.1371/journal.pone.0016081.g001

3 miRNAs (miR-199a-5p, 199b*, 125-5p) was found to be similar while the expression pattern of 11 miRNAs (miR-223, 221, 24, 877, 29b, 29a, 29c, 30c, 365, 148a, and 193) was partially consistent with fibrosis grade [16]. In low graded liver fibrosis, the low expression pattern of 3 miRNAs (miR-140, 27a, and 27b) and the high expression pattern of 6 miRNAs in rat miRNAs (miR-29c*, 143, 872, 193, 122, and 146) in rat miRNA was also similar to our mouse study (GEO Series accession number GSE19865) [11] [12] [17].

The results in this study and previously completed human studies reveal that the expression level of miR-195, 222, 200c, 21, and let-7d was higher in high graded fibrotic liver tissue than in low graded fibrotic liver tissue. Additionally, the expression level of miR-301, 194, and 122 was lower in the high graded fibrotic liver tissue than in low graded fibrotic liver tissue [18] [19] [20](GEO Series accession number GSE16922). This difference in miRNA expression pattern may be contributed to (1) the difference of microarray platform, (2) difference of analytic procedure, and (3) the difference of the species (rat, mouse, and human).

The miR-199 and miR-200 families have are circumstantially related to liver fibrosis. TGFβ-induced factor (TGIF) and SMAD

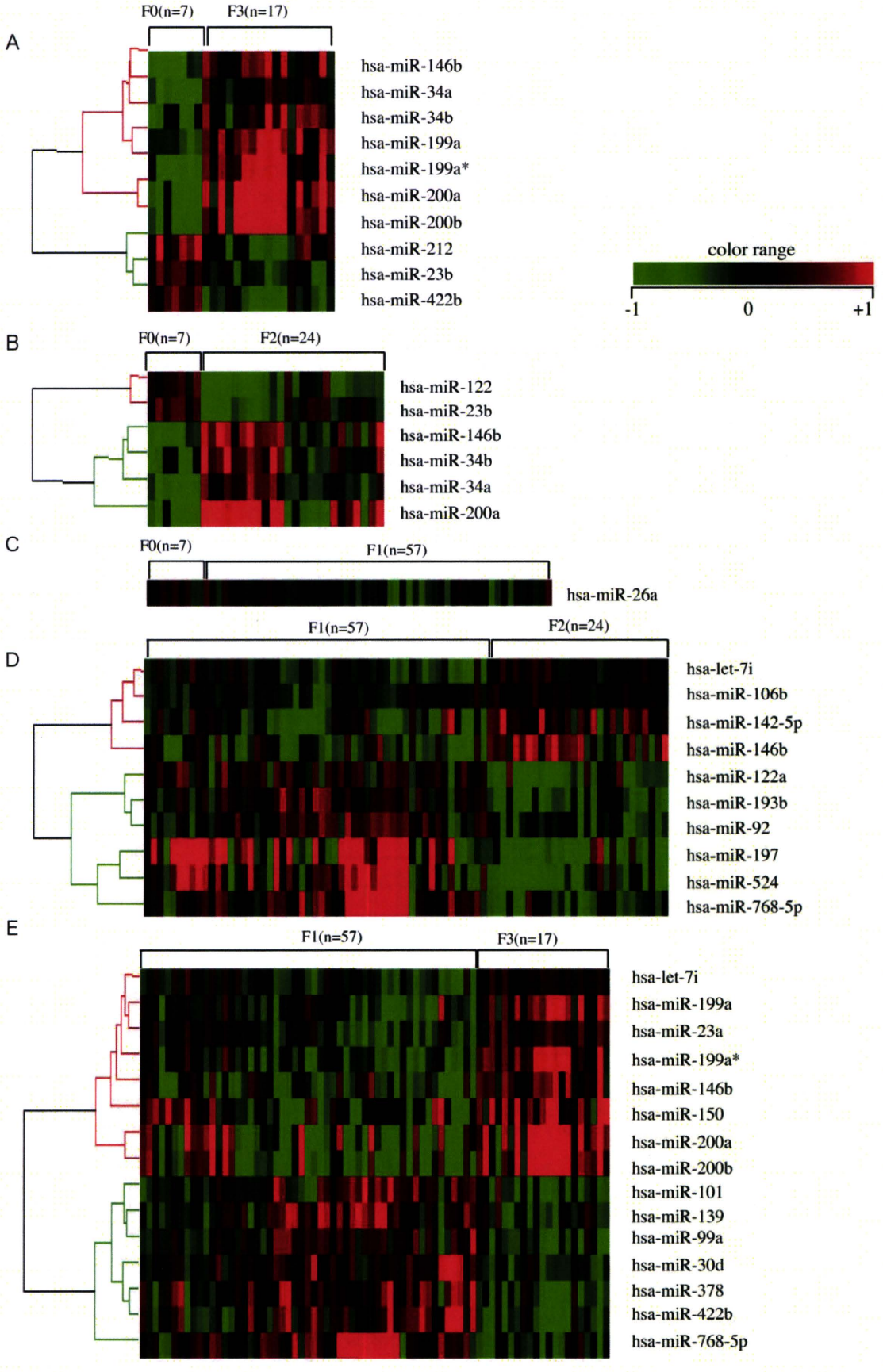
A
F0(n=7)
F3(n=17)
hsa-miR-146b
hsa-miR-34a
hsa-miR-34b
hsa-miR-199a
hsa-miR-199a*
hsa-miR-200a
hsa-miR-200b
hsa-miR-212
hsa-miR-23b
hsa-miR-422b
color range
-1
0
+1
B
F0(n=7)
F2(n=24)
hsa-miR-122
hsa-miR-23b
hsa-miR-146b
hsa-miR-34b
hsa-miR-34a
hsa-miR-200a
C
F0(n=7)
F1(n=57)
hsa-miR-26a
D
F1(n=57)
F2(n=24)
hsa-let-7i
hsa-miR-106b
hsa-miR-142-5p
hsa-miR-146b
hsa-miR-122a
hsa-miR-193b
hsa-miR-92
hsa-miR-197
hsa-miR-524
hsa-miR-768-5p
E
F1(n=57)
F3(n=17)
hsa-let-7i
hsa-miR-199a
hsa-miR-23a
hsa-miR-199a*
hsa-miR-146b
hsa-miR-150
hsa-miR-200a
hsa-miR-200b
hsa-miR-101
hsa-miR-139
hsa-miR-99a
hsa-miR-30d
hsa-miR-378
hsa-miR-422b
hsa-miR-768-5p

Figure 2. Liver fibrosis in human liver biopsy specimen. A. B. C. D. and E. miRNAs whose expression differs significantly between F0 and F3, F0 and F1, F0 and F2, F1 and F2, and F1 and F3, respectively. Relative expression level of each miRNA in human liver biopsy specimen by microarray. Data from microarray were also statistically analyzed using Welch's test and the Bonferroni correction for multiple hypotheses testing. Fold change, p-value are listed in Table S2.
doi:10.1371/journal.pone.0016081.g002

specific E3 ubiquitin protein ligase 2 (SMURF2), both of which play roles in the TGFβ signaling pathway, are candidate targets of miR-199a* and miR-200b, respectively, as determined by the Targetscan algorithm. The expression of miR-199a* was silenced in several proliferating cell lines excluding fibroblasts [21]. Down regulation of miR-199a, miR-199a* and 200a in chronic liver injury tissue was associated with the hepatocarcinogenesis [9]. miR-199a* is also one of the negative regulators of the HCV replication [22]. According to three target search algorithms (Pictar, miRanda, and Targetscan), the miRNAs that may be associated with the liver fibrosis can regulate several fibrosis-related genes (Table S4). Aberrant expression of these miRNAs may be closely related to the progress of the chronic liver disease.

Epithelial-mesenchymal transition (EMT) describes a reversible series of events during which an epithelial cell loses cell-cell contacts and acquires mesenchymal characteristics [23]. Although EMT is not a common event in adults, this process has been implicated in such instances as wound healing and fibrosis. Recent reports showed that the miR-200 family regulated EMT by targeting EMT accelerator ZEB1 and SIP1 [24]. From our observations, overexpression of miR-200a and miR-200b can be connected to the progression of liver fibrosis.

The diagnosis and quantification of fibrosis have traditionally relied on liver biopsy, and this is still true at present. However, there are a number of drawbacks to biopsy, including the invasive nature of the procedure and inter-observer variability. A number of staging systems have been developed to reduce both the inter-observer variability and intra-observer variability, including the METAVIR, the Knodell fibrosis score, and the Scheuer score. However, the reproducibility of hepatic fibrosis and inflammatory activity is not as consistent [25]. In fact, in our study, the degree of fibrosis of the two arbitrary fibrosis groups was classified using the miRNA expression profile with 80% or greater accuracy (data not shown). Thus, miRNA expression can be used for diagnosis of liver fibrosis.

In this study we investigated whether common miRNAs in human and mouse could influence the progression of the liver fibrosis. The signature of miRNAs expression can also serves as a tool for understanding and investigating the mechanism of the onset and progression of liver fibrosis. The miRNA expression profile has the potential to be a novel biomarker of liver fibrosis.

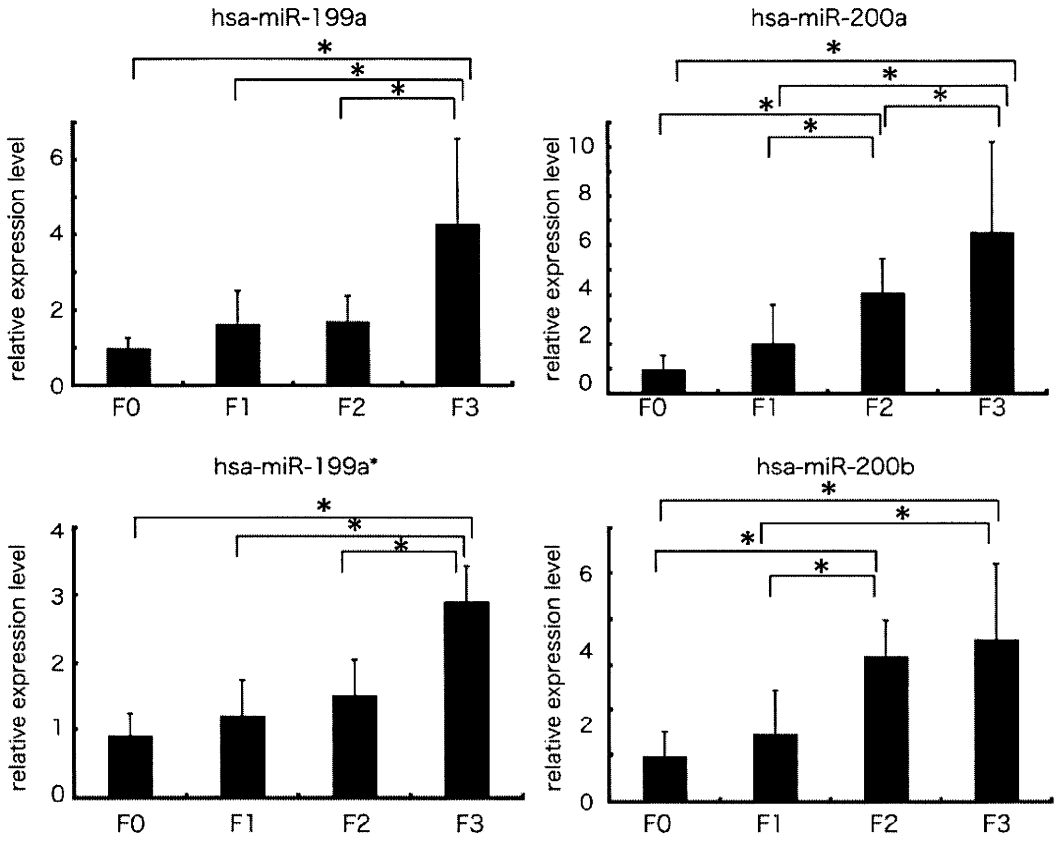

Figure 3. The expression level of miR-199 and 200 families in human liver biopsy specimen by real-time qPCR. Real-time qPCR validation of the 4 miRNAs (miR-199a, miR-199a*, miR-200a, and miR-200b). Each column represents the relative amount of miRNAs normalized to the expression level of U18. The data shown are the means+SD of three independent experiments. Asterisks indicates to a significant difference of $p<0.05$ (two-tailed Student-t test), respectively.
doi:10.1371/journal.pone.0016081.g003

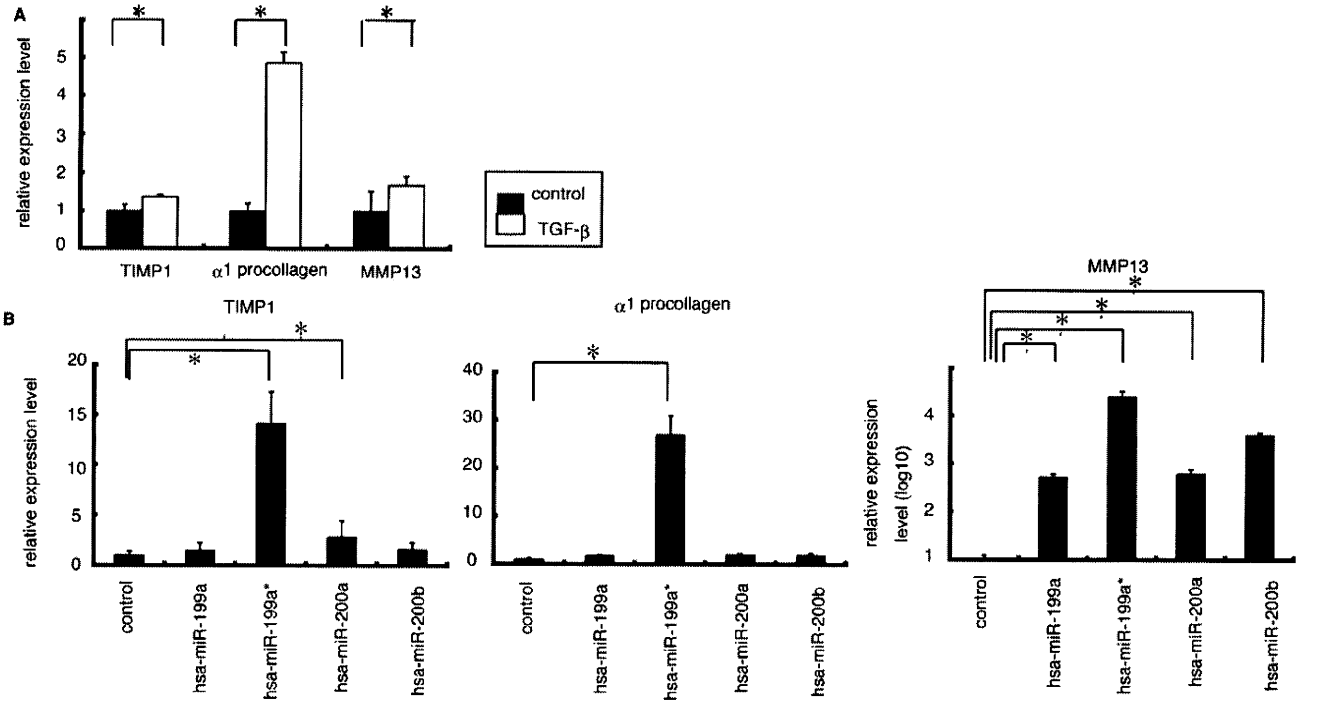

Figure 4. The relationship between expression level of miR-199 and 200 families and expression level of three fibrosis related genes. A. Administration of TGFβ in LX2 cells showed that the expression level of three fibrosis related genes were higher than that in non-treated cells. The data shown are the means+SD of three independent experiments. Asterisk was indicated to the significant difference of $p<0.05$ (two-tailed Student-t test). B. The expression levels of 3 fibrosis related genes in LX2 cells with overexpressing miR-199a, 199a*, 200a, or 200b, respectively were significantly higher than that in cells transfected with control miRNA ($p<0.05$; two-tailed Student t-test).
doi:10.1371/journal.pone.0016081.g004

Moreover miRNA expression profiling has further applications in novel anti-fibrosis therapy in CH.

Materials and Methods

Sample preparation

105 liver tissues samples from chronic hepatitis C patients (genotype 1b) were obtained by fine needle biopsy (Table S1). METAVIR fibrosis stages were F0 in 7 patients, F1 in 57, F2 in 24 and F3 in 17. Patients with autoimmune hepatitis or alcoholic liver injury were excluded. None of the patients were positive for hepatitis B virus associated antigen/ antibody or anti human immunodeficiency virus antibody. No patient received interferon therapy or immunomodulatory therapy prior to the enrollment in this study. We also obtained normal liver tissue from the Liver Transplantation Unit of Kyoto University. All of the patients or their guardians provided written informed consent, and Kyoto University Graduate School and Faculty of Medicine's Ethics Committee approved all aspects of this study in accordance with the Helsinki Declaration.

RNA preparation and miRNA microarray

Total RNA from cell lines or tissue samples was prepared using a *mir*Vana miRNA extraction Kit (Ambion, Austin, TX, USA) according to the manufacturer's instruction. miRNA microarrays were manufactured by Agilent Technologies (Santa Clara, CA, USA) and 100 ng of total RNA was labeled and hybridized using the Human microRNA Microarray Kit protocol for use with Agilent microRNA microarrays Version 1.5 and Mouse microRNA Microarray Kit protocol for use with Agilent microRNA microarrays Version 1.0. Hybridization signals were detected with a DNA microarray scanner G2505B (Agilent Technologies) and the scanned images were analyzed using Agilent feature extraction software (v9.5.3.1). Data were analyzed using GeneSpring GX 7.3.1 software (Agilent Technologies) and normalized as follows: (i) Values below 0.01 were set to 0.01. (ii) In order to compare between one-color expression profile, each measurement was divided by the 75th percentile of all measurements from the same species. The data presented in this manuscript have been deposited in NCBI's Gene Expression Omnibus and are accessible through GEO Series accession number GSE16922 (human) and accession number GSE19865 (mouse).

Real-time qPCR for human miRNA

For detection of the miRNA level by real-time qPCR, TaqMan® microRNA assay (Applied Biosystems) was used to quantify the relative expression level of miR-199a (assay ID. 002304), miR-199a* (assay ID. 000499), miR-200a (assay ID. 000502), miR-200b (assay ID. 002251), and U18 (assay ID. 001204) was used as an internal control. cDNA was synthesized using the Taqman miRNA RT Kit (Applied Biosystems). Total RNA (10 ng/ml) in 5ml of nuclease free water was added to 3 ml of 5× RT primer, 10× 1.5μl of reverse transcriptase buffer, 0.15 μl of 100 mM dNTP, 0.19 μl of RNase inhibitor, 4.16 μl of nuclease free water, and 50U of reverse transcriptase in a total volume of 15 μl. The reaction was performed for 30 min at 16°C, 30 min at 42°C, and 5 min at 85°C. All reactions were run in triplicate. Chromo 4 detector (BIO-RAD) was used to detect miRNA expression.

Animal and Chronic Mouse Liver Injury Model

Each 5 adult (8-week-old) male C57BL/6J mice were given a biweekly intra-peritoneal dose of a 10% solution of CCL_4 in olive oil (0.02 ml/g/ mouse) for the first 4 weeks and then once a week

for the next 4 weeks. At week 4, 6 or 8, the mice were sacrificed. Partial livers were fixed, embedded in paraffin, and processed for histology. Serial liver sections were stained with hematoxylin-eosin, Azan staining, Silver (Ag) staining, and Elastica van Gieson (EVG) staining, respectively. Total RNA from mice liver tissue was prepared as described previously. All animal procedures concerning the analysis of liver injury were performed in following the guidelines of the Kyoto University Animal Research Committee and were approved by the Ethical Committee of the Faculty of Medicine, Kyoto University.

Cell lines and Cell preparation

The human stellate cell lines LX-2, was provided by Scott L. Friedman. LX-2 cells, which viable in serum free media and have high transfectability, were established from human HSC lines [26]. LX-2 cells were maintained in D-MEM (Invitrogen, Carlsbad, CA, USA) with 10% fetal bovine serum, plated in 60 mm diameter dishes and cultured to 70% confluence. Huh-7 and Hela cells were also maintained in D-MEM with 10% fetal bovine serum. HuS-E/2 immortalized hepatocytes were cultured as described previously [27]. LX-2 cells were then cultured in D-MEM without serum with 0.2% BSA for 48 hours prior to TGFβ1 (Sigma-Aldrich, Suffolk, UK) treatment (2.5 ng/ml for 20 hours). Control cells were cultured in D-MEM without fetal bovine serum.

miRNA transfection

LX-2 cells were plated in 6-well plates the day before transfection and grown to 70% confluence. Cells were transfected with 50 pmol of Silencer® negative control siRNA (Ambion) or double-stranded mature miRNA (Hokkaido System Science, Sapporo, Japan) using lipofectamine RNAiMAX (Invitrogen). Cells were harvested 2 days after transfection.

Real-time qPCR

cDNA was synthesized using the Transcriptor High Fiderity cDNA synthesis Kit (Roche, Basel, Switzerland). Total RNA (2 μg) in 10.4 μl of nuclease free water was added to 1 μl of 50mM random hexamer. The denaturing reaction was performed for 10min at 65°C. The denatured RNA mixture was added to 4 μl of 5× reverse transcriptase buffer, 2 μl of 10 mM dNTP, 0.5 μl of 40U/μl RNase inhibitor, and 1.1 μl of reverse transcriptase (FastStart Universal SYBR Green Master (Roche) in a total volume of 20 μl. The reaction ran for 30 min at 50°C (cDNA synthesis), and five min at 85°C (enzyme denaturation). All reactions were run in triplicate. Chromo 4 detector (BIO-RAD, Hercules, CA, USA) was used to detect mRNA expression. The primer sequences are follows; MMP13 s; 5′-gaggctccgagaaatgcagt-3′, as; 5′-atgccatcgtgaagtctggt-3′, TIMP1 s; 5′-cttggcttctgcactgatgg-3′, as; 5′-acgctggtataaggtggtct-3′, α1-procollagen s; 5′-aacatgaccaaaaaccaaaagtg-3′, as; 5′-catt-gtttcctgtgtcttctgg-3′, and β-actin s; 5′-ccactggcatcgtgatggac-3′, as; 5′-tcattgccaatggtgatgacct-3′. Assays were performed in triplicate, and the expression levels of target genes were normalized to expression of the β-actin gene, as quantified using real-time qPCR as internal controls.

Statistical analyses

Statistical analyses were performed using Student's *t*-test; *p* values less than 0.05 were considered statistically significant. Microarray data were also statistically analyzed using Welch's test and Bonferroni correction for multiple hypotheses testing.

Supporting Information

Figure S1 Time line of the induction of chronic liver fibrosis. Upward arrow indicated administration of olive oil or CCl_4. Downward arrow indicates when mice were sacrificed.
(TIF)

Figure S2 Comparison of the expression level of miR-199 and 200 familes in several cell lines and human liver tissue. Endogenous expression level of miR-199a, 199a*, 200a, and 200b in normal liver and LX2 cell as determined by microarray analysis (Agilent Technologies). Endogenous expression level of same miRNAs in Hela, Huh-7 and, immortalized hepatocyte: HuS-E/2 by previously analyzed data [9].
(TIF)

Table S1 Clinical characteristics of patients by the grade of fibrosis.
(DOCX)

Table S2 Extracted human miRNAs related to liver fibrosis.
(DOCX)

Table S3 Corresponding human and mouse miRNAs.
(DOCX)

Table S4 Hypothetical miRNA target genes according to in silico analysis.
(DOCX)

Author Contributions

Conceived and designed the experiments: YM KS. Performed the experiments: YM HT YH NK. Analyzed the data: MT MK. Contributed reagents/materials/analysis tools: YM HT YH NK. Wrote the paper: YM MT AT FM NK TO.

References

1. Wasley A, Alter MJ (2000) Epidemiology of hepatitis C: geographic differences and temporal trends. Semin Liver Dis 20: 1–16.
2. Shepard CW, Finelli L, Alter MJ (2005) Global epidemiology of hepatitis C virus infection. Lancet Infect Dis 5: 558–567.
3. Gressner AM, Weiskirchen R (2006) Modern pathogenetic concepts of liver fibrosis suggest stellate cells and TGF-beta as major players and therapeutic targets. J Cell Mol Med 10: 76–99.
4. Nilsen TW (2007) Mechanisms of microRNA-mediated gene regulation in animal cells. Trends Genet 23: 243–249.
5. Zamore PD, Haley B (2005) Ribo-gnome: the big world of small RNAs. Science 309: 1519–1524.
6. Pillai RS (2005) MicroRNA function: multiple mechanisms for a tiny RNA? Rna 11: 1753–1761.
7. Ura S, Honda M, Yamashita T, Ueda T, Takatori H, et al. (2009) Differential microRNA expression between hepatitis B and hepatitis C leading disease progression to hepatocellular carcinoma. Hepatology 49: 1098–1112.
8. Yamamoto Y, Kosaka N, Tanaka M, Koizumi F, Kanai Y, et al. (2009) MicroRNA-500 as a potential diagnostic marker for hepatocellular carcinoma. Biomarkers 14: 529–538.
9. Murakami Y, Yasuda T, Saigo K, Urashima T, Toyoda H, et al. (2006) Comprehensive analysis of microRNA expression patterns in hepatocellular carcinoma and non-tumorous tissues. Oncogene 25: 2537–2545.
10. Jin X, Ye YF, Chen SH, Yu CH, Liu J, et al. (2008) MicroRNA expression pattern in different stages of nonalcoholic fatty liver disease. Dig Liver Dis.
11. Ogawa T, Iizuka M, Sekiya Y, Yoshizato K, Ikeda K, et al. (2009) Suppression of type I collagen production by microRNA-29b in cultured human stellate cells. Biochem Biophys Res Commun.
12. Ji J, Zhang J, Huang G, Qian J, Wang X, et al. (2009) Over-expressed microRNA-27a and 27b influence fat accumulation and cell proliferation during rat hepatic stellate cell activation. FEBS Lett 583: 759–766.
13. Wienholds E, Kloosterman WP, Miska E, Alvarez-Saavedra E, Berezikov E, et al. (2005) MicroRNA expression in zebrafish embryonic development. Science 309: 310–311.

14. Landgraf P, Rusu M, Sheridan R, Sewer A, Iovino N, et al. (2007) A mammalian microRNA expression atlas based on small RNA library sequencing. Cell 129: 1401–1414.
15. Friedman SL (2008) Hepatic fibrosis-Overview. Toxicology.
16. Roderburg C, Urban GW, Bettermann K, Vucur M, Zimmermann H, et al. (2010) Micro-RNA profiling reveals a role for miR-29 in human and murine liver fibrosis. Hepatology.
17. Venugopal SK, Jiang J, Kim TH, Li Y, Wang SS, et al. (2010) Liver fibrosis causes downregulation of miRNA-150 and miRNA-194 in hepatic stellate cells, and their overexpression causes decreased stellate cell activation. Am J Physiol Gastrointest Liver Physiol 298: G101–106.
18. Jiang J, Gusev Y, Aderca I, Metler TA, Nagorney DM, et al. (2008) Association of MicroRNA expression in hepatocellular carcinomas with hepatitis infection, cirrhosis, and patient survival. Clin Cancer Res 14: 419–427.
19. Jiang X, Tsitsiou E, Herrick SE, Lindsay MA (2010) MicroRNAs and the regulation of fibrosis. Febs J 277: 2015–2021.
20. Marquez RT, Bandyopadhyay S, Wendlandt EB, Keck K, Hoffer BA, et al. (2010) Correlation between microRNA expression levels and clinical parameters associated with chronic hepatitis C viral infection in humans. Lab Invest.
21. Kim S, Lee UJ, Kim MN, Lee EJ, Kim JY, et al. (2008) MicroRNA miR-199a* regulates the MET proto-oncogene and the downstream extracellular signal-regulated kinase 2 (ERK2). J Biol Chem 283: 18158–18166.
22. Murakami Y, Aly HH, Tajima A, Inoue I, Shimotohno K (2009) Regulation of the hepatitis C virus genome replication by miR-199a. J Hepatol 50: 453–460.
23. Gibbons DL, Lin W, Creighton CJ, Rizvi ZH, Gregory PA, et al. (2009) Contextual extracellular cues promote tumor cell EMT and metastasis by regulating miR-200 family expression. Genes Dev 23: 2140–2151.
24. Gregory PA, Bert AG, Paterson EL, Barry SC, Tsykin A, et al. (2008) The miR-200 family and miR-205 regulate epithelial to mesenchymal transition by targeting ZEB1 and SIP1. Nat Cell Biol 10: 593–601.
25. Oberti F, Valsesia E, Pilette C, Rousselet MC, Bedossa P, et al. (1997) Noninvasive diagnosis of hepatic fibrosis or cirrhosis. Gastroenterology 113: 1609–1616.
26. Xu L, Hui AY, Albanis E, Arthur MJ, O'Byrne SM, et al. (2005) Human hepatic stellate cell lines, LX-1 and LX-2: new tools for analysis of hepatic fibrosis. Gut 54: 142–151.
27. Aly HH, Watashi K, Hijikata M, Kaneko H, Takada Y, et al. (2007) Serum-derived hepatitis C virus infectivity in interferon regulatory factor-7-suppressed human primary hepatocytes. J Hepatol 46: 26–36.

Human Molecular Genetics, 2010, Vol. 19, No. 12 **2516–2523**
doi:10.1093/hmg/ddq123
Advance Access published on March 29, 2010

The *FOXE1* locus is a major genetic determinant for radiation-related thyroid carcinoma in Chernobyl

Meiko Takahashi[1,2,†], Vladimir A. Saenko[3,†], Tatiana I. Rogounovitch[4], Takahisa Kawaguchi[1,2], Valentina M. Drozd[5], Hisako Takigawa-Imamura[1], Natallia M. Akulevich[4], Chanavee Ratanajaraya[1], Norisato Mitsutake[4], Noboru Takamura[4], Larisa I. Danilova[6], Maxim L. Lushchik[5], Yuri E. Demidchik[7], Simon Heath[8], Ryo Yamada[1], Mark Lathrop[8,9], Fumihiko Matsuda[1,2,*] and Shunichi Yamashita[3,4]

[1]Center for Genomic Medicine and [2]Institut National de la Santé et de la Recherche Médicale (INSERM) Unit U852, Kyoto University Graduate School of Medicine, Kyoto 606-8501, Japan, [3]Department of International Health and Radiation Research and [4]Department of Molecular Medicine, Atomic Bomb Disease Institute, Nagasaki University Graduate School of Biomedical Sciences, Nagasaki 852-8523, Japan, [5]Department of Thyroid Disease Research, [6]Department of Endocrinology and [7]Belarusian Medical Academy for Postgraduate Education, Minsk 220013, Republic of Belarus, [8]Centre National de Génotypage, Institut Génomique, Commissariat à l'Énergie Atomique, Evry 91000, France and [9]Fondation Jean Dausset-CEPH, Paris 75010, France

Received January 18, 2010; Revised and Accepted March 17, 2010

Papillary thyroid cancer (PTC) among individuals exposed to radioactive iodine in their childhood or adolescence is a major internationally recognized health consequence of the Chernobyl accident. To identify genetic determinants affecting individual susceptibility to radiation-related PTC, we conducted a genome-wide association study employing Belarusian patients with PTC aged 0–18 years at the time of accident and age-matched Belarusian control subjects. Two series of genome scans were performed using independent sample sets, and association with radiation-related PTC was evaluated. Meta-analysis by the Mantel–Haenszel method combining the two studies identified four SNPs at chromosome 9q22.33 showing significant associations with the disease (Mantel–Haenszel *P*: mhp = 1.7×10^{-9} to 4.9×10^{-9}). The association was further reinforced by a validation analysis using one of these SNP markers, rs965513, with a new set of samples (overall mhp = 4.8×10^{-12}, OR = 1.65, 95% CI: 1.43–1.91). Rs965513 is located 57-kb upstream to *FOXE1*, a thyroid-specific transcription factor with pivotal roles in thyroid morphogenesis and was recently reported as the strongest genetic risk marker of sporadic PTC in European populations. Of interest, no association was obtained between radiation-related PTC and rs944289 (mhp = 0.17) at 14p13.3 which showed the second strongest association with sporadic PTC in Europeans. These results show that the complex pathway underlying the pathogenesis may be partly shared by the two etiological forms of PTC, but their genetic components do not completely overlap each other, suggesting the presence of other unknown etiology-specific genetic determinants in radiation-related PTC.

INTRODUCTION

The Chernobyl accident in April 1986 led to radioactive contamination of vast territories in Belarus, Ukraine and Russia. Millions of residents were exposed to a wide spectrum of radionuclides of which ^{131}I was the major dose-forming isotope for the thyroid. A sharp increase in thyroid cancer incidence among those exposed in childhood or adolescence has

*To whom correspondence should be addressed at: Center for Genomic Medicine, Kyoto University Graduate School of Medicine, Yoshida Konoe-cho, Sakyo, Kyoto 606-8501, Japan. Tel: +81 757539313; Fax: +81 757539314; Email: fumi@genome.med.kyoto-u.ac.jp
†These authors contributed equally to this work.

been reported since the early 1990s. Its specific temporal and geographic distribution was suggestive of a common causative event in the development of the malignancy (1,2), which was later proved to be internal exposure to ^{131}I through its incorporation into food chains of pastured cows and further consumption of fresh milk (3). In 2002, the number of diagnosed thyroid cancers in the three most affected countries approached 5000 of which an estimate of 75% could be attributed to Chernobyl radiation (2,4).

Among the variety of histological types of thyroid cancer, only papillary thyroid carcinoma (PTC) displays evident radiation dose–response and accounts for ~95% cases in the Chernobyl aftermath (3,5,6). Radiation is the only known environmental risk factor for PTC seen both after external exposure (7) and internal irradiation (5). The risk for thyroid cancer in the individuals exposed to radiation at young age remains elevated throughout their lifespan. Although a role of predisposing factors commonly associated with sporadic PTC to the female sex is less relevant in cases of radiation-related PTC, a female to male ratio of 1.6 to 1 has been reported (8). Furthermore, radiation-related PTC is also variable in terms of the duration period of latency, the earliest of which is reported to be 4 years (1). It also remains unclear why, notwithstanding the appreciably comparable thyroid radiation doses in Chernobyl PTC patients and in healthy individuals of the same age and of the same settlements (3,9,10), thyroid malignancy develops only in a small fraction of those exposed. Thus, while radiation dose and young age at exposure are well-established risk factors for PTC, observations are suggestive of an existence of genetic factors and complex gene–environment interactions that may modulate individual radiation sensitivity and susceptibility to radiation-related PTC.

In order to identify genetic determinants that modify individual predisposition to radiation-related thyroid malignancy, we conducted a genome-wide association (GWA) study. Two series of genome scans were performed using two independent sample sets consisting of childhood PTC patients of Belarus and control subjects, followed by a validation study using a third set of case and control samples. A total of 667 patients diagnosed for PTC in 1989–2009, and 827 age-matched controls from the same regions were recruited, comprising the largest collection of patients analyzed to date. In addition, genome scan results of 448 Russian DNA samples were also included as general population controls.

RESULTS

GWA study

In the initial genome scan (termed as Study 1), a total of 532 024 autosomal SNP markers of 187 PTC patients and 172 controls were chosen for a case–control association study after quality control of the genotyping results (Table 1). The average call rates per SNP marker and per DNA sample were 0.999 and 0.999, respectively. No strong deviation of inflation factor was observed between the case and control groups (genomic control inflation factor $\lambda = 1.08$, Supplementary Material, Fig. S1a). A statistical analysis comparing genotype distributions did not find SNP markers that showed genome-wide significance. In the subsequent genome scan (termed as Study 2), 214 cases were examined in the association analysis after quality control, and genotype distributions of 509 610 SNP markers were compared with those of 448 Russian population controls. In Study 2, the average call rates per SNP marker and per DNA sample were 0.998 and 0.980, respectively. A slight inflation of genomic control λ-value was observed between the case and control groups (genomic control inflation factor $\lambda = 1.14$, Supplementary Material, Figs S1b and S2), which is most likely due to within-Russia substructures in the Russian population controls. Again, there were no SNP markers that showed genome-wide significance.

A meta-analysis was undertaken through integration of the genotypes obtained in Study 1 and Study 2. Association with radiation-related PTC was evaluated using the Mantel–Haenszel method for 506 840 SNP markers that passed quality control in both studies. The distribution of the mhp-values along the chromosomes is shown in Figure 1. A slight inflation of λ-value was observed between case and control ($\lambda = 1.11$, Supplementary Material, Fig. S1c). A cluster of four SNPs at chromosome 9q22.23 showed genome-wide significance ($P < 5.0 \times 10^{-8}$), namely, rs925489, rs7850258, rs965513 and rs10759944 with meta-analysis P-values of 1.7×10^{-9}, 1.7×10^{-9}, 4.9×10^{-9} and 3.5×10^{-9}, respectively (Fig. 2 and Table 2). These markers are in strong linkage disequilibrium (LD) to each other (pairwise $D' > 0.999$, $r^2 > 0.999$). Although there were no neighboring SNPs showing stronger signals (Supplementary Material, Table S1), nine other markers at the same chromosomal locus showed suggestive association signals ($mhp = 5.2 \times 10^{-4}$ to 1.4×10^{-6}) (Table 2). In addition, we examined the association by pooling genotypes obtained in Studies 1 and 2. After correction for population stratification using Eigenstrat as well as for residual inflation by the genomic control method, all four markers that showed genome-wide significance in the meta-analysis were slightly below the level of genome-wide significance (rs7850258: $P = 1.5 \times 10^{-7}$, rs925489: $P = 1.5 \times 10^{-7}$, rs10759944: $P = 2.4 \times 10^{-7}$, rs965513: $P = 3.2 \times 10^{-7}$).

SNP markers located on the X chromosome were tested for association in a separate analysis. Cases and controls were sub-grouped into males and females and association analysis was carried out. As a result, none of the markers showed genome-wide significance ($mhp > 3.6 \times 10^{-5}$ for males, $mhp > 1.6 \times 10^{-5}$ for females).

Validation study

The 425-kb region between rs4742698 and rs4618817 encompassing these markers was evaluated for LD structure with the genotyping results of Study 1 and Study 2. Three LD blocks were identified: block A between rs4742698 and rs16924042, block B between rs1512261 and rs10818094 and block C between rs7871887 and rs4618817. All of the four most significant markers are in block B (Fig. 2). There are eight genes that have been localized in the vicinity of these SNPs: *TMOD1* (Entrez Gene ID: 7111), *C9orf97* (ID: 158427), *NCBP1* (ID: 4686), *XPA* (ID: 7507), *KRT18P13* (ID: 392371), *FOXE1* (ID: 2304), *C9orf156* (ID: 51531) and

Table 1. Specification of the DNA samples used for the study

Study	Sample set	Classification	Number	Age at exposure Range	Age at exposure Mean ± SD	Age at diagnosis Range	Age at diagnosis Mean ± SD
Study 1	PTC1	Cases	187	0 – 17	3.0 ± 3.8	3 – 20	10.0 ± 4.1
	CTR1	Controls	172	0 – 17	1.5 ± 2.8	—	—
Study 2	PTC2	Cases	214	0 – 17	5.8 ± 5.2	2 – 22	13.9 ± 5.5
	CTR2	Controls[a]	448	—	—	—	—
Study 3	PTC3	Cases	259	0 – 18	6.8 ± 5.5	3 – 22	16.5 ± 4.4
	CTR3	Controls	648	0 – 26	6.2 ± 5.9	—	—

[a]Russian population controls from other genetic studies.

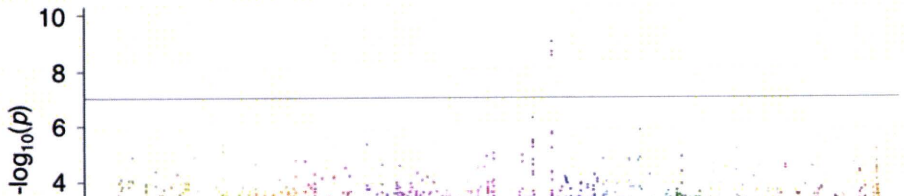

Figure 1. Manhattan plot of the combined GWAS results for Studies 1 and 2. *P*-values calculated by the Trend χ^2 test for 506 840 autosomal SNPs are plotted in $-\log_{10}$ scale with respect to their chromosomal positions. The horizontal line indicates Bonferroni-adjusted $P = 9.6 \times 10^{-8}$.

HEMGN (ID: 55363), but none of these genes reside in block B. Seven out of the nine markers showing suggestive association signals are located at either 5′ or 3′ flanking region of the *FOXE1* gene in block C. In addition, an imputation analysis was performed for SNP markers in blocks A, B and C using genotypes of International HapMap Project as reference. We identified three additional SNPs in block B, namely rs7030280, rs10983700 and rs1588635, located approximately 9–11 kb centromeric to rs925489, showing similar levels of association (imputed $P = 2.8 \times 10^{-9}$ for rs7030280 and rs10983700, imputed $P = 3.7 \times 10^{-9}$ for rs1588635) (Supplementary Material, Table S2). No other SNP markers in block A or block C reached genome-wide significance.

This region at 9q22.23 containing the *FOXE1* (or *TTF2*) gene which encodes a thyroid-specific transcription factor was recently identified as a chromosomal locus strongly associated with predisposition to sporadic thyroid cancer in an Icelandic study (11). Among the seven SNPs showing significant associations ($P < 2.8 \times 10^{-9}$) in the Icelandic sporadic PTC patients, rs965513 was strongest ($P = 6.8 \times 10^{-20}$, OR = 1.77) (Table 2). We therefore selected rs965513 located ~57 kb upstream to *FOXE1* for further genotyping by Taqman using an independent sample set (termed as Study 3) of 259 cases and 648 controls (Table 1). The strong association ($P = 2.0 \times 10^{-4}$) was reproduced and was further reinforced when the genotypes of the three studies were combined for meta-analysis (mhp $= 4.8 \times 10^{-12}$, OR = 1.65, 95% CI: 1.43–1.91).

Very recently, another genetic study focusing on 97 candidate genes mediating thyroid carcinogenesis identified rs1867277 in the 5′-UTR of *FOXE1* as a genetic determinant for sporadic PTC ($P = 5.9 \times 10^{-9}$, OR = 1.49, 95% CI: 1.30–1.70) (12). Since rs1867277 was not examined in our study, we designed a Taqman probe and genotyped 660 PTC cases (PTC1, PTC2 and PTC3) and 820 Belarusian controls (CTR1 and CTR3) (Table 1). A significant association was obtained with a *P*-value of 4.5×10^{-7} and OR of 1.48 (95% CI: 1.27–1.71).

Genotyping of rs944289 at chromosome 14q13.3

Rs944289 at chromosome 14q13.3 showed the second strongest association with sporadic PTC in the Icelandic population ($P = 2.5 \times 10^{-8}$, OR = 1.44, 95% CI: 1.26–1.63) (11). This SNP is located in a 249-kb LD region which does not contain any known genes, but it lies close to *TTF1* (ID: 7080), another thyroid-specific transcription factor gene. We investigated whether rs944289 showed significant association in our genome scan results. Of our interest, it failed to show any association with radiation-related PTC ($P = 0.23$ in Study 1, $P = 0.43$ in Study 2 and mhp = 0.17 by meta-analysis) (Table 2).

Correlation between rs965513 genotypes and disease latency

It is considered that thyroid cancer requires an induction and latency period of at least 10 years after exposure to ionizing radiation (13). We divided the 660 case samples into two groups depending on the date of diagnosis being either within, or more than, 10 years since radiocontamination.

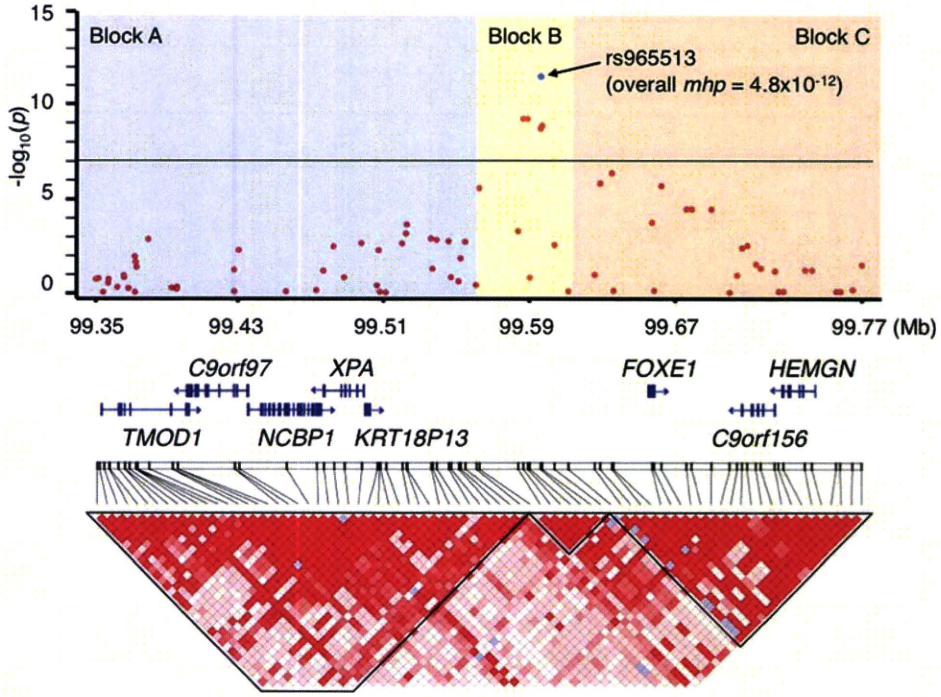

Figure 2. A schematic organization of the human *FOXE1* locus at 9q22.23 with the genome scanning results. Mhp-values calculated by the Trend χ^2 test in $-\log_{10}$ scale were plotted in red circles for SNPs located in the 425-kb region between rs4742698 and rs4618817 at chromosome 9q22.23. The blue circle indicates mhp-value of rs965513 by meta-analysis using the combined results of Study 1 to Study 3. The structure and orientation of eight genes in the region were shown below the plots with their transcriptional orientations according to NCBI Reference Sequence Build 36.3. LD blocks were generated according to pairwise LD estimates of the SNPs located within the region using the genome scan results of Study 1 and Study 2.

For the early-onset group, there were 178 patients aged 3–25 years (mean age ± SD: 11.2 ± 4.3 years) who were diagnosed within the first 10 years (before 1997), with latency of 7.0 ± 1.9 years. For the late-onset group, there were 482 samples aged 10–39 years (22.9 ± 7.5 years) who were diagnosed after 1997, with latency of 16.4 ± 3.8 years. Looking at the results for rs965513, there was a much stronger association observed for the early-onset cases ($P = 2.0 \times 10^{-9}$, OR = 1.97, 95% CI: 1.58–2.47) than the late-onset cases ($P = 6.0 \times 10^{-8}$, OR = 1.52, 95% CI: 1.31–1.77) when compared with 1268 controls (CTR1 to CTR3). However, there was no statistical significance to prove the stronger impact of rs965513 on the early-onset of PTC (p-heterogeneity = 0.063).

DISCUSSION

In this study, we have undertaken a GWA study of radiation-related PTC employing Belarusian patients and control subjects. We identified four markers in strong LD at chromosome 9q22.23 that were significantly associated with the disease. The strong association was further evident by selecting one of these markers, rs965513, with the genotyping of an independent set of samples by Taqman (overall mhp = 4.8×10^{-12}, OR = 1.65, 95% CI: 1.43–1.91). Rs965513 was recently identified as a genetic risk factor for sporadic PTC in individuals of European descent (11) and is located within an LD block which lies centromeric to *FOXE1*.

Another recent report showed a strong association of rs1867277 at the 5′-UTR of *FOXE1* with the risk of differentiated thyroid cancer, in particular with the classic variant of PTC. *FOXE1* is a thyroid-specific DNA binding protein recognizing binding sites on thyroglobulin and thyroperoxidase genes expressed in thyroid follicular cells (14,15). Although the precise role of *FOXE1* in PTC remains to be fully established, this study provides further evidence of *FOXE1* involvement in thyroid carcinogenesis. Rs1867277 is so far the only functional variant associated with sporadic PTC identified within the *FOXE1* gene, and the risk allele (A) augmented *FOXE1* transcription by creation of a binding site for USF1 and USF2 transcription factors. The fact that stronger association signals were observed for SNPs outside block C containing *FOXE1* in both the Icelandic and Belarusian studies may indicate the existence of DNA sequences in block B with unknown function acting cooperatively with rs1867277. Certainly, however, we cannot rule out the involvement of other genes in the region.

Although the association of rs965513 with PTC was stronger in the early-onset cases than in the late-onset cases, the difference was not statistically significant (p-heterogeneity = 0.063). Short latency was reported to be often associated with more aggressive tumors with prominent local invasion and distant metastases (16). However, it is difficult to directly associate our results to such morphological features since the environmental background of patients, including individual thyroid radiation dose and detailed clinical information are not available.

Individual susceptibility to thyroid cancer is considered to be complex involving the interaction of low-penetrance genes and the environment. Here we provide the first evidence

Table 2. Results of association analysis for SNP markers at 9q22.33 and 14q13.3 using the Chernobyl childhood thyroid cancer cohort

Marker	Allele[a]		Chr	Position	Statistics by study					Study 1 + 2		Study 1 + 2 + 3		Gudmundsson *et al.*			
	Ref.	Var			Study	Freq var. Case	Control	Trend P[b]	OR (95% CI)[c]	Mhp[d]	OR (95% CI)[c]	Mhp[d]	OR (95% CI)[c]	Freq var. Case	Control	P-value[e]	OR (95% CI)[c]
rs1512261	G*	T	9	99562351	1	0.500	0.419	0.029	1.39 (1.03, 1.87)	6.9×10^{-6}	1.53 (1.27, 1.84)						
					2	0.509	0.391	5.2×10^{-5}	1.62 (1.28, 2.04)								
rs1877432	G*	A	9	99583701	1	0.706	0.610	0.010	1.53 (1.12, 2.09)	5.2×10^{-4}	1.40 (1.16, 1.69)						
					2	0.697	0.628	0.016	1.36 (1.06, 1.74)								
rs925489	C*	T	9	99586421	1	0.487	0.334	3.3×10^{-5}	1.89 (1.40, 2.55)	1.7×10^{-9}	1.79 (1.48, 2.16)						
					2	0.481	0.349	6.0×10^{-6}	1.73 (1.37, 2.18)								
rs7850258	A*	G	9	99588834	1	0.487	0.334	3.3×10^{-5}	1.89 (1.40, 2.55)	1.7×10^{-9}	1.79 (1.48, 2.16)						
					2	0.481	0.349	6.0×10^{-6}	1.73 (1.37, 2.18)								
rs965513	A*	G	9	99595930	1	0.487	0.334	3.3×10^{-5}	1.89 (1.40, 2.55)	4.9×10^{-9}	1.76 (1.45, 2.12)	4.8×10^{-12}	1.65 (1.43, 1.91)	0.490	0.352	6.8×10^{-20}	1.77 (1.57, 2.00)
					2	0.476	0.352	1.7×10^{-5}	1.68 (1.33, 2.12)								
					3	0.462	0.367	2.0×10^{-4}	1.48 (1.20,1.83)								
rs10759944	A*	G	9	99596793	1	0.487	0.334	3.3×10^{-5}	1.89 (1.40, 2.55)	3.5×10^{-9}	1.77 (1.46, 2.14)			0.490	0.352	1.7×10^{-19}	1.77 (1.57, 2.01)
					2	0.479	0.352	1.2×10^{-5}	1.69 (1.34, 2.14)								
rs7848973	A*	G	9	99628660	1	0.503	0.392	0.0032	1.56 (1.16, 2.10)	2.5×10^{-6}	1.56 (1.29, 1.87)						
					2	0.502	0.393	2.0×10^{-4}	1.56 (1.24, 1.97)								
rs7024345	A*	G	9	99635059	1	0.380	0.305	0.038	1.39 (1.02, 1.90)	1.4×10^{-6}	1.63 (1.33, 1.98)			0.387	0.285	1.9×10^{-12}	1.58 (1.39, 1.80)
					2	0.397	0.273	4.0×10^{-6}	1.75 (1.37, 2.23)								
rs1443434	G*	T	9	99657300	1	0.487	0.392	0.012	1.47 (1.09, 1.97)	2.6×10^{-4}	1.41 (1.17, 1.70)			0.488	0.385	2.8×10^{-9}	1.52 (1.32, 1.74)
					2	0.477	0.398	0.0070	1.37 (1.09, 1.73)								
rs907580	T*	C	9	99662418	1	0.374	0.314	0.10	1.30 (0.96, 1.78)	5.7×10^{-6}	1.58 (1.30, 1.92)			0.395	0.281	1.1×10^{-14}	1.66 (1.46, 1.89)
					2	0.396	0.273	4.2×10^{-6}	1.74 (1.37, 2.23)								
rs925487	C*	T	9	99676219	1	0.463	0.372	0.015	1.45 (1.08, 1.96)	4.5×10^{-5}	1.47 (1.22, 1.77)			0.472	0.359	2.6×10^{-13}	1.60 (1.41, 1.81)
					2	0.465	0.369	9.2×10^{-4}	1.48 (1.17, 1.88)								
rs10984103	A*	C	9	99679096	1	0.463	0.372	0.015	1.45 (1.08, 1.96)	4.6×10^{-5}	1.47 (1.22, 1.77)			0.472	0.359	2.2×10^{-13}	1.59 (1.41, 1.81)
					2	0.465	0.369	9.5×10^{-4}	1.48 (1.17, 1.87)								
rs7866436	G*	A	9	99689917	1	0.465	0.369	0.010	1.49 (1.10, 2.00)	5.2×10^{-5}	1.47 (1.22, 1.76)						
					2	0.463	0.372	0.0016	1.46 (1.15, 1.84)								
rs944289	C	T*	14	35718997	1	0.626	0.580	0.23	1.21 (0.90, 1.63)	0.17	1.13 (0.95, 1.36)			0.644	0.558	2.5×10^{-8}	1.44 (1.26, 1.63)
					2	0.607	0.584	0.43	1.10 (0.87, 1.40)								

SNP markers in blocks B and C with $P < 1 \times 10^{-3}$ are shown for 9q22.23. Rs944289 on 14q13.3 which also showed significant association in the Icelandic study was included. A complete list of the markers in the 425-kb region with statistical results is shown in Supplementary Material, Table S1.

[a]The reference (ref.) and variant (var.) alleles refer to NCBI Build 36.3 and the risk allele is indicated with an asterisk.

[b]The P-values using Trend χ^2 test are shown.

[c]Odds ratio (OR) is calculated for the risk allele with a confidence interval (CI) of 95%.

[d]The Trend χ^2 Mantel–Haenszel P-values are shown.

[e]The P-values using a standard likelihood ratio χ^2 statistic are shown.

that the risk of developing PTC after internal radiation exposure is largely associated with the genetic determinant conferring risk for human thyroid malignancies in the general population. However, *FOXE1* is unlikely to be the only key player in radiation-related thyroid carcinogenesis and it remains to be established whether or not radiation-related PTC has other etiology-specific genetic components for inherited predisposition. Rs944289 at chromosome 14q13.3 strongly associated with sporadic PTC in the Icelandic population was not significant in our results. Moreover, in our GWA study, two additional SNPs with meta-analysis *P*-value being smaller than 1×10^{-6} were identified, of which one was on chromosome 9p and the other on chromosome 12p. Since neither of these chromosomal loci have been identified as being associated with sporadic PTC, they may be potential candidates for susceptibility loci specific to radiation-related PTC. These observations clearly suggest that different genetic components are involved in carcinogenesis of sporadic and radiation-related PTC.

Only a few case–control studies to identify genetic risk factors of radiation-related thyroid cancer have been reported to date. Three studies included Chernobyl PTC (17–19) and thyroid cancers in an occupationally exposed cohort (20). A recent article examined the genetic determinants in the patients with radiation-related thyroid nodules (21). The possibilities of association between the risk for PTC after radiation exposure and *TP53* (ID: 7157) (17,18), *RET* (ID: 5979) (20) or *XRCC1* (ID: 7515) (20) were demonstrated. However, most of these studies had a limited sample size and insufficient gene coverage. Apart from the *TP53* Arg72Pro polymorphism (rs1042522) being associated with the risk of radiation-related PTC in adult patients (17,18), the findings were not replicated in independent sample sets. None of the SNP markers that were significant in the above studies were on the Illumina array. According to HAPMAP, rs25487 (*XRCC1*) and rs1800858 (*RET*) are in complete LD ($D' = 1$, $r^2 = 1$) with rs1799778 and rs2505535, respectively, which are both on the array. However, the associations were negative for both markers in our study ($P = 0.94$ for rs1799778 and $P = 0.03$ for rs2505535).

MATERIALS AND METHODS

Study populations

A total of 667 patients (174 males and 493 females, sex ratio 0.35) diagnosed for thyroid cancer in 1989–2009 were recruited. Inclusion criteria for cases were as follows: (i) age at the time of Chernobyl accident 0–18 years old, including those *in utero*, in April–June 1986, who were (ii) residing at the time in the radiocontaminated regions of Belarus and (iii) histologically verified diagnosis of PTC. Demographic and diagnostic information was retrieved from Thyroid Cancer Center (Minsk, Belarus). At the moment of exposure, 378 patients were residents of Gomel region of Belarus which is the most radiocontaminated area in the country, 195 patients were from Brest region, 10 from Mogilev region and 84 were from other radiocontaminated regions of the country.

As control subjects, a total number of 620 healthy individuals (165 males and 455 females, sex ratio 0.36) were recruited. Inclusion criteria for controls were: (i) age at the time of accident between 0 and 18 years old, including those *in utero*, in April–June 1986, who were (ii) residing at the time in the radiocontaminated regions of Belarus, (iii) euthyroid state and (iv) no thyroid cancer by the time of sampling (February 2006 to April 2009). At the time of possible radiation exposure, 574 healthy participants were residents of Brest region, 34 of Gomel region, 11 of Mogilev region and one individual from another region. According to the radioecological and radiation epidemiology studies, all cases and 620 controls are considered to have received thyroid doses ranging 21–1500 mGy (22,23). Additional DNA samples of 207 individuals who were: (i) born after 1987 (79 samples), (ii) older than 18 years of age at the time of accident (three samples) or (iii) considered to have been exposed to a negligible amount, if any, of radiation according to their residential information (125 samples), were also utilized for the studies as representative Belarusian population controls. Demographic and residential information was obtained by personal inquiry, and peripheral blood samples were collected in the contaminated regions during bi-annual thyroid screening programs (which also included neck ultrasound and consultation of endocrinologist) of Belarusian population. Euthyroid state was confirmed by laboratory tests being 1.64 ± 1.57 μU/ml for thyrotropin (normal range 0.5–5.0 μU/ml) and 1.17 ± 0.28 ng/dl for free thyroxin (normal range 0.7–1.55 ng/dl) in the whole control group. The absence of thyroid cancer was met by selecting only those individuals without detectable thyroid nodules on ultrasound. For Study 2, the genotypes of 448 Russian controls were used as population controls (24). The Institutional Review Board and the Ethics Committee of each institution approved the protocols used. All participants were fully informed of the purpose and procedures, and a written consent was obtained.

DNA preparation

DNA was extracted from peripheral blood mononuclear cells using Puregene kit (Qiagen, Germantown, MD, USA) according to the manufacturer's protocol. DNA concentration and purity were measured with a Nanodrop 1000 spectrophotometer (Thermo Scientific, Waltham, MA, USA). The samples were stored at −80°C until use.

GWA study

Two series of genome scans were performed using two independent sample sets. 194 cases and 179 controls, and 214 cases and 448 Russian population controls, were used in the first and second genome scans (Study 1 and Study 2), respectively. Validation of genome scan results (Study 3) was performed by Taqman analysis using a third independent sample set consisting of 259 cases and 648 controls.

Study 1: genome scan. A total of 567 512 autosomal SNPs were genotyped in 194 thyroid cancer patients and 179 controls with Illumina Human610-Quad BeadChip on a BeadStation 500G Genotyping System, and genotype calls were generated and summary files were made using the Bead Studio version 3.1.3.0 software package (Illumina, Inc., San

Diego, CA, USA). Quality control procedures were systematically performed for the genome scan results. Initially, two control samples with call rates being smaller than 90% were removed from the analysis. Subsequently, degrees of kinship between individuals were examined by Pi-hat in PLINK, a multidimensional scaling method (25). For seven pairs of cases and five pairs of controls showing high degrees of kinship (PI-HAT > 0.3), the sample with the lower call rate was excluded. Principal component analysis by 'smartpca' in EIGENSOFT (26) including HAPMAP phase II samples confirmed no deviation in all DNA samples from Caucasian population. Following the quality control for SNP markers, a total of 35 488 markers were excluded due to low call rates (lower than 95%), a low minor allele frequency (smaller than 0.01) or significant distortion from Hardy–Weinberg equilibrium (P-value smaller than 10^{-7}). After these steps, 532 024 SNP markers of 187 PTC patients (mean age $\pm$ SD: 3.0 ± 3.8 years) and 172 controls (1.5 ± 2.8 years) were used for statistical analyses.

Association of SNP markers on the X chromosome was examined in a separate analysis. The same criteria for QC were applied and 16 448 SNP markers were used to test disease association between 58 cases and 60 controls for males, and 128 cases and 111 controls for females.

Study 2: genome scan. In 214 thyroid cancer patients (mean age $\pm$ SD: 5.8 ± 5.2 years), 567 512 autosomal SNPs were genotyped using the same SNP arrays as those used in Study 1. Genotype calls of 448 Russian DNA samples were used as population-based controls. The same exclusion criteria as Study 1 were applied for the quality control, but no DNA samples were removed from the analysis. After removing 57 902 SNP markers that fit the exclusion criteria, a total of 509 610 SNP markers were used for statistical analyses. Analysis of the X chromosome was performed as described for Study 1, in 52 cases and 235 controls for males and in 161 cases and 213 controls for females.

Study 3: validation analysis. Validation of genome scan results was carried out in 259 cases (mean age $\pm$ SD: 6.8 ± 5.5 years) and 648 controls (mean age $\pm$ SD: 6.2 ± 5.9 years) using the Taqman SNP assays (Applied Biosystems, Foster City, CA, USA) according to the manufacturer's guidelines. A predesigned and functionally tested probe was used for rs965513 (C_1593670_20, Applied Biosystems), and a custom designed probe by the same producer was used for rs1867277.

Statistical analysis

A case–control association in each study was examined using trend χ^2 test to compare genotypic distributions between cases and controls (27). Population stratification was assessed by the genomic control method (28). Meta-analysis of genome scan results was carried out with trend mode of the Mantel–Haenszel method (29), by combining the genotypes of Study 1 and Study 2 for 506 840 autosomal SNP markers that passed quality control in both studies. The genotypes for the autosomal SNPs obtained in Studies 1 and 2 were pooled, and population stratification was corrected by Eigenstrat (26) followed by the genomic control method. Meta-analysis of 16 448 SNP markers on the X chromosome was performed for Study 1 males and Study 2 males, as well as for Study 1 females and Study 2 females.

The overall significance level of rs965513 was calculated by meta-analysis using the Mantel–Haenszel method, combining the genotypes of Study 1 to Study 3. The LD structure was derived using the genotypes of Study 1 and Study 2 using the Haploview software (30) by calculating pairwise LD indices (D' and r^2) between SNP markers in the region.

Imputation of missing genotypes was performed using MACH 1.0 (http://www.sph.umich.edu/csg/abecasis/MaCH/index.html). The genotype data of CEU (CEPH European) obtained from the Phase III HapMap database (draft2) were used as reference and the 425-kb region between rs4742698 and rs4618817 was examined for association. In the process of imputation, 50 Markov chain iterations were implemented.

SUPPLEMENTARY MATERIAL

Supplementary Material is available at *HMG* online.

ACKNOWLEDGEMENTS

We would like to thank all the study participants who made this project possible. The Russian Control Data came from three studies: KMSU: A.V. Polonikov, V.P. Ivanov, M.A. Solodilova; TOMSK: M.B. Freidin, V.P. Puzyrev, L.M. Ogorodova; UFA: E.K. Khusnutdinova, A.S. Karunas, Y.Y. Fedorova. We also thank M. Kokubo, M. Palomares, M. Aksornworanart and M. Mizutani for technical assistance, and A. Yoshizumi, H. Uneme and K. Hirosawa for informatics management.

Conflict of Interest statement. None declared.

FUNDING

This work was supported in part by Nagasaki University Global COE Program and by 'Grants-in-Aid for Young Scientists' from the Ministry of Education, Culture, Sports, Science and Technology (Japan). The funders had no role in study design, data collection and analysis, decision to publish or preparation of the manuscript.

REFERENCES

1. Kazakov, V.S., Demidchik, E.P. and Astakhova, L.N. (1992) Thyroid cancer after Chernobyl. *Nature*, **359**, 21.
2. Bennett, B., Repacholi, M. and Carr, Z. (2006) *Report of the UN Chernobyl Forum Expert Group 'Health'*, WHO Press, Geneva.
3. Cardis, E., Kesminiene, A., Ivanov, V., Malakhova, I., Shibata, Y., Khrouch, V., Drozdovitch, V., Maceika, E., Zvonova, I., Vlassov, O. *et al.* (2005) Risk of thyroid cancer after exposure to 131I in childhood. *J. Natl Cancer Inst.*, **97**, 724–732.
4. Tronko, M.D., Howe, G.R., Bogdanova, T.I., Bouville, A.C., Epstein, O.V., Brill, A.B., Likhtarev, I.A., Fink, D.J., Markov, V.V., Greenebaum, E. *et al.* (2006) A cohort study of thyroid cancer and other thyroid diseases after the chornobyl accident: thyroid cancer in Ukraine detected during first screening. *J. Natl Cancer Inst.*, **98**, 897–903.
5. Williams, D. (2002) Cancer after nuclear fallout: lessons from the Chernobyl accident. *Nat. Rev. Cancer*, **2**, 543–549.